Search for the Dalitz Decay of the Higgs Boson in p-p Collisions with the CMS Detector

PhD Thesis Proposal

Luisa Fernanda Chaparro Sierra

Advisor
Juan Carlos Sanabria Arenas, PhD.

Co-advisor
Camilo Andrés Carrillo Montoya, PhD.

Universidad de Los Andes
Department of Physics
Bogotá D.C., Colombia.

Geneva, Switzerland, July 2013

Contents

Summary **3**

Introduction **4**

1 State of the Art **5**
1.1 The Electroweak Symmetry Breaking in the Standard Model. 5
1.2 Higgs Boson Production at LHC 6
1.3 Higgs Boson Decay Channels 7
1.4 Higgs Bosons in Models Beyond the Standard Model 12

2 The CMS Experiment **12**
2.1 The CMS Detector 14
2.1.1 The Tracker System 15
2.1.2 Electromagnetic Calorimeter ECAL 15
2.1.3 Hadronic Calorimeter HCAL 16
2.1.4 Muon System 16
2.1.5 Trigger and DQM System 19
2.2 Higgs Physics in CMS 20
2.2.1 $H \to \gamma\gamma$ 20
2.2.2 $H \to ZZ$ 21
2.2.3 $H \to W^+W^-$ 22
2.2.4 $H \to \tau^+\tau^-$ 23
2.2.5 $H \to b\bar{b}$ 24
2.2.6 $H \to Z\gamma$ 25

3 The Dalitz Decay $H \to \gamma\gamma* \to \gamma l^+l^-$ **27**

4 Goals **31**
4.1 General Goals 31
4.2 Specific Goals 31

5 Timetable **32**

References **34**

Summary

This document presents the proposal for my PhD dissertation in Physics. The main focus of my research will be the search of the Dalitz decay of the Higgs boson in different final states and the measurement of their branching ratio. This study will be performed using the data collected in 2012 by the CMS experiment, during the proton-proton collision run of the LHC at the center-of-mass energy of 8 TeV. The Dalitz decay channel of the Higgs boson corresponds to the Higgs decaying into two gammas, one real and another one virtual ($H \to \gamma\gamma^*$). The virtual photon will convert into a fermion-antifermion pair ($\gamma^* \to f\bar{f}$). The "cleanest" experimental signature will come from the gamma star coupling with leptons, therefore the search for this decay will focus on muons and electrons. The decay to tau leptons will not be included in this study due to the complex nature of their decays, which make them hard to identify from the experimental point of view. In summary, the Dalitz decay of the Higgs boson corresponds to $H \to \gamma l^+ l^-$. This signature is similar to the one of a Higgs boson decaying into a γ and a Z boson, where the Z boson decays into two leptons. However, these two processes will be easily distinguishable since in the $H \to \gamma\gamma^*$ the reconstructed invariant mass of the two leptons is expected to be $\leq$ 20 GeV while in the $H \to \gamma Z$ the leptons mass is expected to be around the mass of the Z boson, 90 GeV.

Recently, two of the LHC experiments, CMS and ATLAS, have announced clear observations of a Higgs boson with a mass of 125-126 GeV [1–3]. Due to the coupling of the Higgs boson to any massive particle, it has many decay channels, the strongest ones been those involving coupling to the most massive particles; therefore, the phenomenology of the "Higgs sector" of the Standard Model (SM) is very rich. The measurement of the Higgs mass has "fixed" the parameters of the Higgs potential providing concrete values for observables such as branching ratios and decay widths (within the framework of the SM). Detail measurements of any Higgs observable are instead crucial to study the underlying dynamics. Since the photon is massless, the Higgs boson does not couple to it directly (at tree level), it only does it through loops of heavy charged particles like W's or top quarks. This has two important consequences for the $H \to \gamma\gamma$ decay channel: the branching ratio of this channel is not too small, even though it is a second order process; and it is sensitive to the presence of loops of massive charge particles that can contribute to the invariant amplitude of the process. The same arguments apply to the $H \to Z\gamma$, $H \to \gamma\gamma^*$ channels. In conclusion, the coupling of the Higgs boson to neutral vector bosons can be seen as an indirect way to search for massive charge particles Beyond the SM (BSM).

In supersymmetric models (SUSY) the simplest version of the Higgs sector includes five particles: three with a neutral electric charge, one with positive and one with negative electric charge. In some parametrization of the Minimal Standard SUSY Model (MSSM) the lightest neutral Higgs will have practically the same properties of the SM Higgs, making it very difficult to distinguish the phenomenology of the Higgs sector of SM and MSSM. However, the contributions of charged Higgs bosons, charginos and sfermions to the $H \to \gamma\gamma$, γZ, $\gamma\gamma^*$ could be looked for in a detailed study of these channels.

In order to perform the proposed analysis, events with high p_T gammas and dileptons ($\mu^+\mu^-$, e^+e^-) will be selected, demanding small invariant masses for the dileptons (in order to separate the $H \to \gamma\gamma^*$ from the $H \to \gamma Z$ channel). The invariant mass of the three particles will be around 125 GeV (the mass of the Higgs). The main source of events that mimic our signal of interest (background), come from Drell-Yang (DY) processes resulting in two leptons with small invariant mass, accompanied by the independent emission of a high p_T gamma. Another source of background would be the same DY process accompanied by a jet misidentified by the detector as a photon. These backgrounds could be reduced drastically by kinematic selection criteria because in the events from signal the dilepton and the photon are expected to be produced in opposite directions (back-to-back) in the parton-parton center of mass frame, while in most backgrounds this will not be the case. In order to determine how well the backgrounds can be removed, detailed Monte Carlo (MC) studies should be performed. From the analysis of the data and the MC studies at 8 TeV, information could be inferred in order to perform detailed MC studies at 14 TeV, the expected center of mass energy for the next run of the LHC. At 14 TeV, the yields for the $H \to \gamma\gamma$, γZ, $\gamma\gamma*$ will make these channels very relevant, both, for understanding of the Higgs sector of the SM, and to search for any possible evidence of physics BSM.

Introduction

On July of 2012 the spokesmen of CMS and ATLAS experiments announced at CERN the discovery a neutral boson with a mass around 125 GeV and decay channels consistent with those of the SM Higgs boson. On March of 2013 at the *Rencontres du Moriond* Conference new evidence gathered by both experiments allowed to identify the new boson with the Higgs boson, putting an end to a search that had started 30 years ago, right after the discovery of the W and Z vector bosons by the UA1 and UA2 experiments of the S$p\bar{p}$S collider at CERN, announced in 1983. At that time the experimental confirmation of the existence of massive electroweak vector bosons represented the definitive consolidation of the Standard Model of Particles and Fields. This model relied upon the spontaneous symmetry breaking of the $SU(2) \times U(1)$ gauge symmetry of the electromagnetic and weak interactions, mediated by a neutral scalar field via a mechanism that has come to be known as the "Higgs mechanism". The presence of this scalar field and its coupling to the matter fields allowed the inclusion of mass terms for bosons and fermions, while preserving the gauge invariance, and therefore the renormalizability of the model. The great phenomenological success of this theory, that eventually became known as *The Standard Model*, is exemplified by the discovery of the W and Z just as predicted. The very important role played by the scalar boson (Higgs boson) in providing mass for the other fields and preserving the necessary gauge symmetry made its search the most important and urgent problem in physics since 1983.

The mass of the Higgs boson in the SM is a free parameter therefore its value was practically unconstrained by the theory, making its experimental search difficult, since a wide range of energies had to be scanned. The initial searches were performed at the S$p\bar{p}$S accelerator at CERN with negative results. Next came the Tevatron at Fermilab in 1988 colliding protons and antiprotons with the center-of-mass energy of 2 TeV. During the 1990's the electron-positron collider LEP of CERN joined the search but without any positive outcome. Finally, in 2010 the Large Hadron Collider (LHC) at CERN started its operations colliding protons at a center-of-mass energy of 7 TeV, and by 2012 at 8 TeV. The first hints of a scalar boson where announced on december of 2011 and were confirmed by July of 2012. By 2013 the strong evidence convinced the particle physics community that the discovered particle was the Higgs.

The two experiments that performed the initial search for the Higgs at the LHC were CMS and ATLAS. In the scientific goals of those experiments, and of the whole LHC project, the main priority was the search and discovery of the Higgs boson. The CMS experiment concentrated on five channels: $H \to \gamma\gamma$, $H \to ZZ$, $H \to W^+W^-$, $H \to \tau^+\tau^-$ and $H \to b\bar{b}$.

The initial announcements of the Collaboration were based on the first three channels, that have the highest signal yields and the lowest background contamination. By the time of the Moriond conference the $H \to \tau^+\tau^-$ analysis also provided a signal. Currently, the effort of the experiment is focusing in channels with lesser yields and/or higher backgrounds like $H \to b\bar{b}$, $H \to Z\gamma$.

The High Energy Physics Group of Universidad de los Andes is a member of the CMS Collaboration since 2006. As a PhD student in Physics at Universidad de los Andes, and a member of High Energy Physics Group, I am also part of the CMS Collaboration, and I have been working directly at CERN since January of 2012. Any member of this collaboration acquires responsibilities at three levels: hardware, software and physics. Our group works in the operation of the RPC muon detectors at the level of hardware, in muon reconstruction at the level of software and in the search of "Exotic" physics, search for SUSY signals and Higgs physics. I work on the Higgs physics and belong to the analysis group dedicated to the study of the $H \to Z\gamma$ channel. Within that group I have focus my study in the $H \to \gamma\gamma^* \to \gamma l^+l^-$ (Dalitz decay). Even though the Dalitz decay channel is actually a radiative process associated with the $H \to \gamma\gamma$ channel, its experimental signature is similar to the $H \to Z\gamma \to l^+l^-\gamma$ and therefore it is being studied by the "$HZ\gamma$" group.

As a member of the CMS $HZ\gamma$ analysis group, I will study the Higgs Dalitz decay as the main subject of my PhD dissertation using the data at 8 TeV, but also performing studies of this channel for the future run of the LHC at 14 TeV. As part of my duties as a member of CMS I will continue working on the operation of the RPC muon detectors. This work will be relevant for my thesis, since the Dalitz decay of the Higgs will result in electrons or muons, and it will be necessary to perform detail studies of muon reconstruction and trigger

efficiencies (for instance).

This document is organized in the following way: section 1 presents the state of the art of the Higgs physics at the LHC; next, in section 2, a brief description of the CMS experiment, its detector and the Higgs physics program is presented; in section 3 the details of the proposed Higgs Dalitz decay analysis are discussed; the goals and the timetable of the proposal are listed in sections 4 and 5.

1 State of the Art

1.1 The Electroweak Symmetry Breaking in the Standard Model.

The Standard Model of Particles (SM) is the best theoretical framework for the description of the dynamics of particles and interactions at the most fundamental level that we understand up to now. The main ingredients of the SM are:

- It is a quantum-mechanical theory
- It is a relativistic theory
- It gives a quantum-mechanical treatment to the interactions (it is a quantum filed theory).
- It is a gauge field theory
- It describes the electromagnetic, weak and strong interactions.
- It is a renormalizable theory

The electromagnetic and strong sectors of the SM can be described in terms of "pure" gauge field theories, Quantum Electrodynamics (QED) in the electromagnetic case and Quantum Chromodynamics (QCD) in the strong interaction case. That means that QED is a gauge field theory based on the symmetry group $U(1)_{EM}$, and QCD is a gauge field theory based on the symmetry group $SU(3)_C$. As a result of this character, the interaction fields are massless: the photon field for QED and eight gluon fields for QCD. The gauge invariance of these theories guarantees their renormalizability. Massive interaction fields would break the gauge invariance and make the theories non-renormalizable.

The experimental evidence collected up to the 1950's for the weak interaction suggested that it was mediated by massive vector fields, charged and neutral; therefore, this interaction could not be described by a simple pure gauge field theory. Even more, the discovery of parity violation by the weak interaction demanded a separation of the quiralities of the matter fields (fermion fields). The mass terms associated with the matter fields mix quiralities, and therefore also break any gauge invariance associated with the weak interaction. In conclusion, the situation by the end of the 1950's was that, due to the weak interaction, no quantum fields could have mass!, nor the interaction neither the matter fields, otherwise the theory would be non-re-normalizable.

The solution to this problem came in the form of the inclusion of a neutral scalar field with a degenerated vacuum state, the Higgs field. The field coupled to the matter fields through Yukawa terms. The spontaneous symmetry breaking of the Higgs vacuum state would generate the coupling of the matter fields to the non-zero vacuum expectation value, generating effective mass terms for this fields. The implementation of the symmetry breaking also resulted in massive and non-massive vector fields (interaction fields); the resulting massive fields were $W^{\pm}$ and Z^0, and the massless field was γ. The theory turned out to be re-normalizable, solving the problem of the mass terms, and unifying the electromagnetic and weak interactions. The mass terms of all massive fields are the result of the interaction with the vacuum of the Higgs field. The Higgs field should also be massive, and should interact with any massive field with a strength dependent on the mass of the field.

The discovery of neutral-current interactions in the 1970's, evidence of the Z^0, and later, at the beginning of the 1980's, the direct observation of $W^{\pm}$ and Z^0, consolidated the SM as the model for the electro-weak and strong interactions. The theory was renormalizable and very successful phenomenologically, but depended on

the existence of a massive and neutral scalar field with positive parity, the Higgs field. The Higgs should interact with any other massive field, and the coupling should depend on the mass of the field. Unfortunately the SM could not make a prediction of the mass of the Higgs, therefore the experimental search had to be driven by m_H, an unknown parameter, making it much more difficult.

The Higgs of the SM has several couplings which, in experimental terms, means that there are several production and decay channels. The very precise measurements of the electroweak sector of the SM, specially those performed at LEP in the 1990's, where such that if m_H became known, cross sections and branching ratios for the Higgs production and decay would be pre-determined with high enough accuracy. The discovery of a scalar state with a mass of ~ 125 GeV, announced in July of 2012 by the experiments ATLAS and CMS, and the latter updates that indicate to a high confidence level that it has spin 0 and positive parity, as well as couplings that depend on the mass of the state to which it is coupling, suggest very strongly that this state has all the features of the SM Higgs [4]. Therefore, one could fix $m_H = 125$ GeV, and have predictions for cross sections and branching ratios for the different Higgs channels. Any significant deviations from these values could represent important indications of physics beyond the SM. The detailed study of each and every one of the experimental Higgs channels becomes very important to understand the electroweak symmetry breaking mechanism of the SM, and what lies beyond.

1.2 Higgs Boson Production at LHC

The SM predicts that the Higgs bosons could be produced in a number of ways, although the probability of any of these production channels in proton-proton collisions in the energy range of the TeV is very small; for example, only 1 Higgs boson per 10 billion collisions in the case of the Large Hadron Collider [5]. The main production mechanisms are associated to the fact that the Higgs boson couples preferentially to heavy particles, like W and Z vector bosons, top and bottom quarks. The Feynman diagrams associated to the main Higgs boson production mechanisms are presented in figure 1 [6].

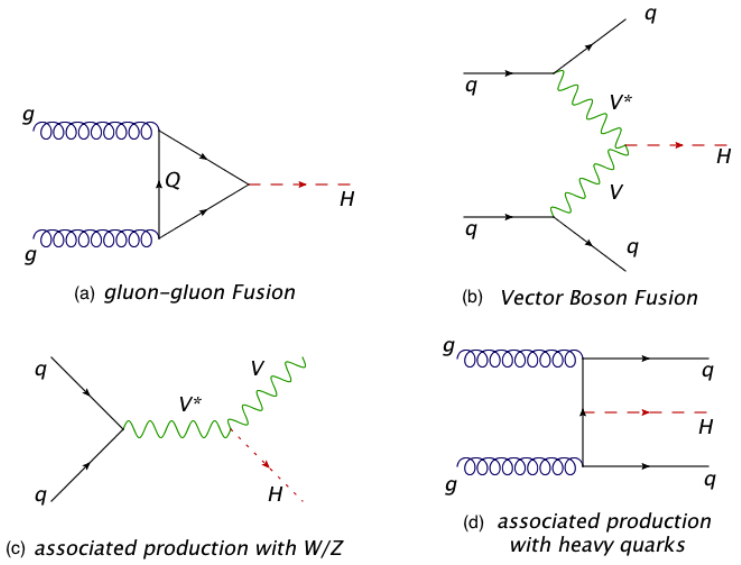

Figure 1: The dominant SM Higgs boson production mechanism at LHC [6].

The most important mechanism is the gluon fusion process (see figure 1 a), where the Higgs boson is produced from the coupling of two gluons mediated by a loop of heavy fermions. Since the coupling of particles to the Higgs boson is proportional to their mass, the main contributions to the fermionic loop comes from the heaviest quarks. In practice it is enough to consider the contributions of top and bottom quarks. A smaller contribution, with a rate that is roughly one order of magnitude lower, comes from the vector boson fusion (VBF) processes, where the Higgs boson is produced, at tree-level, by two vector bosons, leaving as distinct signature the debris

of two high energy quarks with a large gap in rapidity between them [6, 7].

The production of the Higgs through gluon fusion is sensitive to a fourth generation of quarks. Because the Higgs couples in proportion to the fermion mass, a heavier generation of quarks is not suppressed in the process as would be expected for a process associated to a heavier particle (this argument is indeed valid for any heavy fermions). This has the consequence that the Higgs cross section is sensitive to a fourth generation of quarks even if the quarks are too heavy for a direct discovery at the LHC. The mass range is limited by the scale of new physics where the standard model breaks down [5, 6].

Vector boson fusion is another possibility when two partons exchange Ws or Zs which fuse producing a Higgs boson (see figure 1 b). The colliding fermions do not need to be of the same type. For a Higgs of 125 GeV this process is the second most important production mechanism.

Higgs bosons can be produced also in association with Z or W bosons via a process called "Higgs-strahlung" (see figure 1 c). When an elementary fermion collides with an anti-fermion, the two can merge to form a virtual W or Z boson which, if it carries sufficient energy, can then emit a Higgs boson. At the LHC this process is the third largest.

The final process that is commonly considered is the top quark fusion (see figure 1 d). This process involves two colliding gluons, each of them producing a $t\bar{t}$ pair. The t from one gluon and the $\bar{t}$ from the other one combine to form a Higgs boson [5].

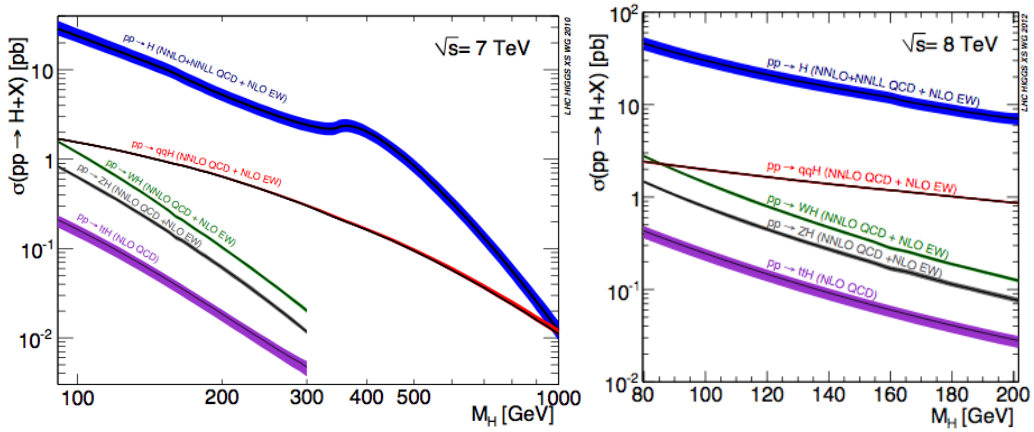

Figure 2: LHC Higgs boson production cross sections at a center of mass energy of (left) 7 TeV [6]. (right) 8 TeV[3].

The main LHC Higgs production cross sections at a center of mass energy of 7 and 8 TeV are shown in figure 2 (left) and (right) respectively. In conclusion, at the LHC energies the main production mechanism is gluon fusion, but other production channels had significant contributions, and by looking at the topology of the whole event one can achieve a level of identification of these channels.

1.3 Higgs Boson Decay Channels

Until July of 2012 the Higgs boson was the only fundamental particle predicted by the SM that had not been observed by the experiments. One of the problems in its search was that the theory did not predict the mass of the state. Since the Higgs boson couples to other states thought their mass, the set of decay modes depends on m_H.

The search of the Higgs boson was one of the main goals of the CMS and ATLAS experiments. Both experiments focused on five main decay channels: $H \to \gamma\gamma$, $H \to ZZ \to 4l$, $H \to WW \to 2l2\nu$, $H \to \tau\tau$ followed by at least one leptonic τ decay; and $H \to b\bar{b}$ followed by b-quark fragmentation into jets. The most recent results, presented in Moriond 2013 by CMS and ATLAS, reported an excess of events around 125 GeV

in several channels corresponding to their 2011 and 2012 datasets at 7 and 8 TeV respectively, confirming the announcement of the discovery of a Higgs-like boson from july of 2012.

The channels mentioned above are important by themselves but also because they have the largest branching fractions or signal to background ratios, therefore, in terms of search and discovery they were the main channels. Other channels with low sensitivity, like: $t\bar{t}H$,$H \to b\bar{b}$; W/ZH, $H \to \tau\tau$, W/ZH, $H \to WW \to 2l2\nu$, $H \to ZZ \to 2l2q$, demand more complex analysis, as well as larger statistics, but physics wise they are also very important. Some of these channels are excellent candidates to show possible deviations from the SM predictions, and might open the door to the observation of physics beyond the SM.

For a given value of m_H, search sensitivity depends on the production cross section, the decay branching ratio into the selected final state, the signal selection efficiency, the mass resolution and the level of background of similar or identical final state topologies.

Decay Mode	Production tagging	# of subchannels	m_H range (GeV)	Int Lum. (fb^{-1}) 7TeV	8 TeV
$\gamma\gamma$	untagged dijet (VBF)	4 1or 2	110-150	5.1	5.3
ZZ	untagged	3	110-600	5.1	5.3
WW	untagged dijet (VBF)	4 1or 2	110-600	4.9	5.1
$\tau\tau$	untagged dijet (VBF)	16 4	110-145	4.9	5.1
$b\bar{b}$	lepton, E_T^{miss}(VH)	10	110-135	5.0	5.1

Table 1: Summary of the sub-channels used by CMS in the analysis of each decay mode.

Combining the Higgs boson search results requires a simultaneous analysis of the data selected by the individual decay modes, accounting for their correlations and for all the statistical and systematic uncertainties. The statistical methodology used in this combination was developed by the ATLAS and CMS Collaborations in the context of the LHC Higgs Combination Group [2, 3, 8, 9].

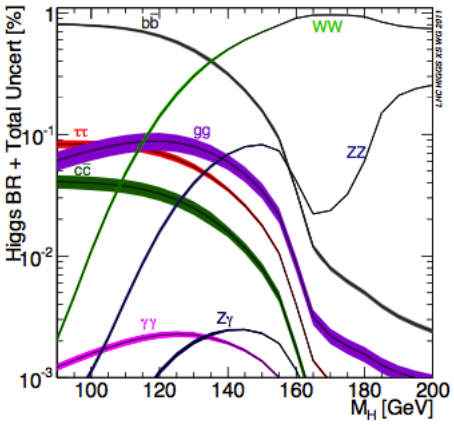

Figure 3: Branching fractions as a function of the Higgs boson mass. The width of the lines represents the total theoretical uncertainty [1].

The magnitude of a possible Higgs boson signals is characterized by relevant branching fractions, on production cross sections, on the expectation of the standard model, denoted (σ/σ_{SM}) and referred as the signal strength. The predicted branching fractions for a Higgs boson as a function of Higgs boson mass are shown in figure 3.

In the $H \to \gamma\gamma$ analysis, the SM Higgs boson signal was searched for in a simultaneous statistical analysis of the diphoton invariant-mass distributions for eleven exclusive event classes: five classes (four untagged and one VBF-tagged) for the 7 TeV data and six classes (four untagged and two VBF-tagged) for the 8 TeV data. Figure 4 shows that the $H \to \gamma\gamma$ search has reached the sensitivity for excluding the SM Higgs boson at 95% CL in the mass range 110-144 GeV, while the observed data exclude it in the following three mass ranges: 113-122 GeV, 128-133 GeV, and 138-149 GeV. All diphoton analysis give observed exclusion limits near $m_H = 125$ GeV that are much weaker than the expected for the background, which implies a significant excess of events with diphoton masses around 125 GeV. The consistency of the results obtained with the three alternative approaches confirms the robustness of the measurement. In conclusion the $H \to \gamma\gamma$ channel shows evidence of a new state that decays into two photons with an invariant mass of 125 GeV, with a CL well beyond 95% (confirming previous announcements).

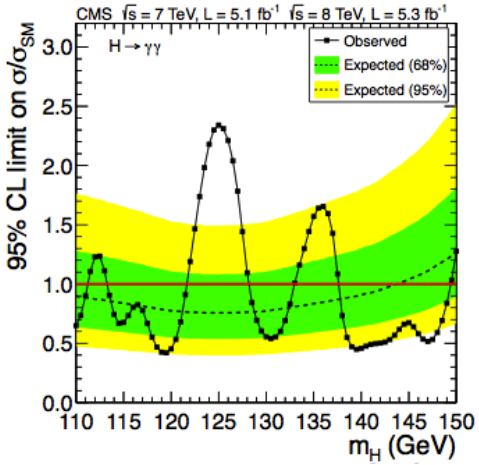

Figure 4: The 95% CL upper limits on the production cross section of a Higgs boson expressed in units of the SM Higgs boson production cross section, σ/σ_{SM}, as obtained in the $H \to \gamma\gamma$ search channel for the baseline analysis [3].

In the $H \to ZZ \to 4l$ analysis, the SM Higgs boson signal was searched for in a simultaneous statistical analysis of six 2D distributions of the four-lepton invariant mass m_{4l}. The six distributions correspond to the three lepton final states (4e, 4μ, 2e2μ) and the 7 and 8 TeV datasets.

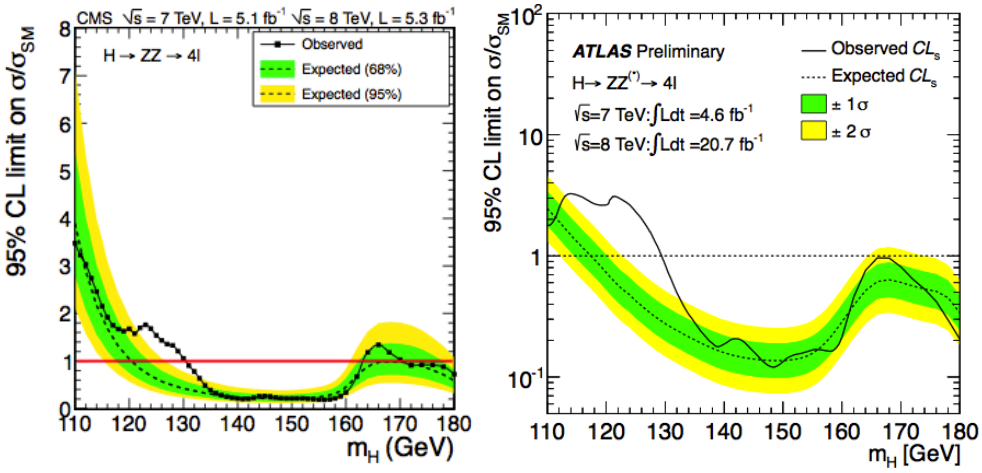

Figure 5: The 95% CL upper limits on the production cross section of a Higgs boson expressed in units of the SM Higgs boson production cross section, σ/σ_{SM}, for the $H \to ZZ \to 4l$. (left) CMS results. [3]. (right) ATLAS results [10].

Figure 5 (left) shows the 95% CL upper limits on the Higgs boson production cross section. The $H \to ZZ \to 4l$ search has reached the sensitivity for excluding the SM Higgs boson at 95% CL in the mass range 120-180 GeV, while the observed data exclude it in the following two mass ranges: 130-164 GeV and 170-180 GeV. The observed exclusion limits for $m_H = 120 - 130$ GeV are much weaker than the expected limits for the background, suggesting a significant excess of four-lepton events in this mass range. Figure 5 (right) shows that the observed exclusion starts only at around 130 GeV due to the excess at 125 GeV. As a cross-check, statistical analysis using only the m_{4l} distributions has been performed. The results are found to be consistent with the 2D analysis, although with less sensitivity.

In the $H \to WW \to l\nu l\nu$ analysis, the SM Higgs boson signal is searched for in a simultaneous statistical analysis of eleven exclusive final states: same flavor (e^+e^- and $\mu^+\mu^-$) dilepton events with 0 and 1 jet for the 7 and 8 TeV datasets; different flavor $e^\pm\mu^\mp$ dilepton events with 0-jet and 1-jet for the 7 and 8 TeV datasets, dilepton events in the VBF-tag category for the 7 TeV dataset, and same flavor and different flavor dilepton events in the VBF-tag category for the 8 TeV dataset.

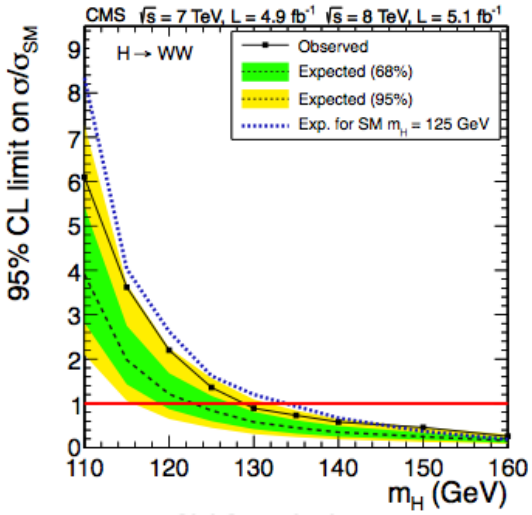

Figure 6: The 95% CL upper limits on the production cross section of a Higgs boson expressed in units of the SM Higgs boson production cross section, σ/σ_{SM}, for the $H \to WW \to l\nu l\nu$ [3].

Figure 6 shows the 95% CL upper limits on the Higgs boson production cross section. The $H \to WW \to l\nu l\nu$ search has reached a sensitivity for excluding the SM Higgs boson at 95% CL in the mass range 122-160 GeV, while the observed data exclude it in the mass range 129-160 GeV. The observed exclusion limits are weaker than the expected ones for the background, suggesting an excess of events in the data corresponding to a masses less than 130 GeV. However, given the mass resolution of about 20% in this channel, owing to the presence of the two undetectable neutrinos, a broad excess is observed across the whole mass range from 110 to 130 GeV. The observed limits in this channel are consistent with the expectation for a SM Higgs boson at $m_H = 125$ GeV.

In the $H \to \tau^+\tau^-$ channel, the 0-jet, 1-jet, and VBF categories are used to set 95% CL upper limits on the Higgs boson production. The ditau system is reconstructed in four final states: $e\tau_h$, $\mu\tau_h$, $e\mu$, $\mu\mu$, where the leptons come from $\tau \to e\nu\nu$ or $\tau \to \mu\nu\nu$ decays. The 0-jet and 1-jet categories are further split into two categories of low or high ditau transverse momentum. The 7 and 8 TeV data are treated independently giving a total of 40 ditau mass distributions. Figure 7 shows the 95% CL upper limits on the Higgs boson production cross section in this channel. The $H \to \tau^+\tau^-$ search has not yet reached the SM Higgs boson exclusion sensitivity; the expected limits on the signal event rates are 1.3-2.4 times larger than the event rates expected for the SM Higgs boson in this channel.

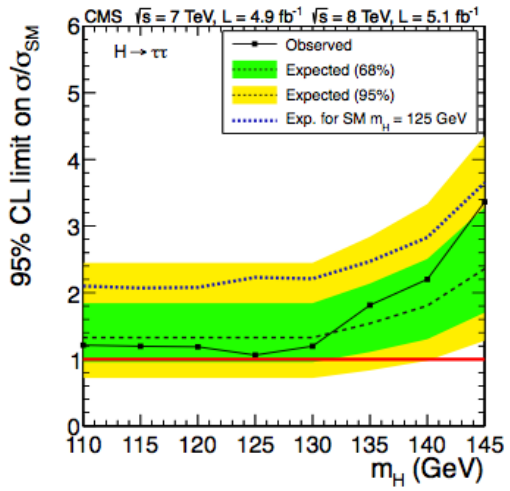

Figure 7: The 95% CL upper limits on the production cross section of a Higgs boson expressed in units of the SM Higgs boson production cross section, σ/σ_{SM}, for the $H \to \tau^+\tau^-$ [3].

In the $H \to b\bar{b}$ analysis, five final states are considered: two b-tagged jets with E_T^{miss} ($Z \to \nu\nu$); e^+e^-; $\mu^+\mu^-(Z \to l^+l^-$); e+E_T^{miss}, and $\mu + E_T^{miss}$ ($W \to l\nu$). Each of these categories is further split into two categories of low or high $b\bar{b}$ transverse momentum. The 7 and 8 TeV data are treated independently. Figure 8 shows the 95% upper CL limits on the Higgs boson production cross section in this channel. The $H \to b\bar{b}$ search has not yet reached the SM Higgs boson exclusion sensitivity; the expected limits on the signal event rates are 1.2-2.8 times larger than the event rates expected for the SM Higgs boson in this channel.

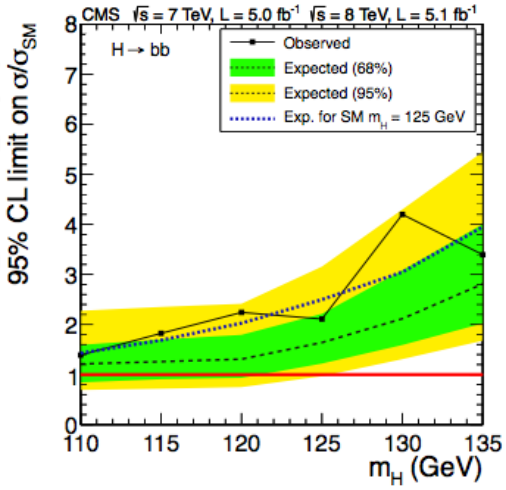

Figure 8: The 95% CL upper limits on the production cross section of a Higgs boson expressed in units of the SM Higgs boson production cross section, σ/σ_{SM}, for the $H \to b\bar{b}$ [3].

The five individual search channels described above are combined into a single search for the SM Higgs boson. The largest contributions to the overall excess are from the $\gamma\gamma$ and $ZZ \to 4l$ channels. Both channels have good mass resolution and allow for a precise measurement of the mass of the resonance corresponding to the excess. Their combined significance is 5.0σ.

Table 2 summarizes the median expected and observed local significance for a SM Higgs boson mass of 125.5 GeV, from the individual decay modes and their combinations. All the results are consistent, within their

uncertainties, with the expectations for the SM Higgs boson. In section 2.2 all of these channels will be explained in more detail in the case of CMS experiment.

Decay Mode or combination	Expected (σ)	Observed (σ)
ZZ	3.8	3.2
$\gamma\gamma$	2.8	4.1
WW	2.5	1.6
$b\bar{b}$	1.9	0.7
$\tau^+\tau^-$	1.4	–
$\gamma\gamma$ +ZZ	4.7	5.0
WW+$\tau^+\tau^-$ +$b\bar{b}$	3.4	1.6
$\gamma\gamma$ +ZZ +WW+$\tau^+\tau^-$ +$b\bar{b}$	5.8	5.0

Table 2: The median expected and observed significances of the excesses in the individual decay modes and their various combinations for a SM Higgs boson mass at 125 GeV.

1.4 Higgs Bosons in Models Beyond the Standard Model

The data available on the Higgs boson decay has already imposed constrains, not only on the properties of the SM version of the state, but on any composed nature of this particle in other models. However, the results presented by CMS and ATLAS at the Moriond Conference still leave the door open to several alternatives of physics BSM, including many SUSY-inspired models. In minimal SUSY models the simplest version of the Higgs sector includes five particles: three neutral ones and two charged ones. In some parametrization of the Minimal Standard SUSY Model (MSSM) the lightest neutral Higgs will have practically the same properties of the SM Higgs, making it very difficult to distinguish the phenomenology of the Higgs sector of SM and that one of the MSSM.

Since the couplings of the Higgs to all the other SM particles becomes known once its mass is available, the branching ratios for the different decay modes are also determined. Any significant departure from the expected values for these observables could give us the hint for the emergence of physics BSM. The coupling of the Higgs to other particles is proportional to the mass of the states (and the data has already shown that [4]), therefore the contribution of massive charged Higgs bosons, charginos and sfermions to the loops that generate the couplings between the neutral Higgs boson and the neutral vector-bosons: $H \to \gamma\gamma$, γZ, $\gamma\gamma^*$, could be looked for in a detailed study of these channels. The statistics available for these processes at 8 TeV may not be enough to draw definitive conclusions about evidences of physics BSM, but its study will be very important when data at 14 TeV becomes available.

2 The CMS Experiment

The CMS Experiment is one of the four experiments at the Large Hadron Collider (LHC), the particle accelerator located at CERN in the border between France and Switzerland. The LHC is a proton-proton collider designed to reach collision energies that could go up to 14 TeV. The LHC is installed inside a tunnel, originally built for the LEP accelerator, with a circumference of 26.7 km. The LHC can also collider heavy-Ions (Lead-Lead).

Each proton beam of the LHC was designed to reach an energy up to 7 TeV, equivalent to a center of mass energy of 14 TeV for every collision. Currently it collides beams of protons with a center of mass energy of 8 TeV. In each of the rings, bunches of protons will travel in opposite directions crossing in four points along the circumference. In each of this interaction points there is a large particle detector. In point 1 ATLAS, in point 2 ALICE, in point 5 CMS and in point 8 LHCb (see figure 9).

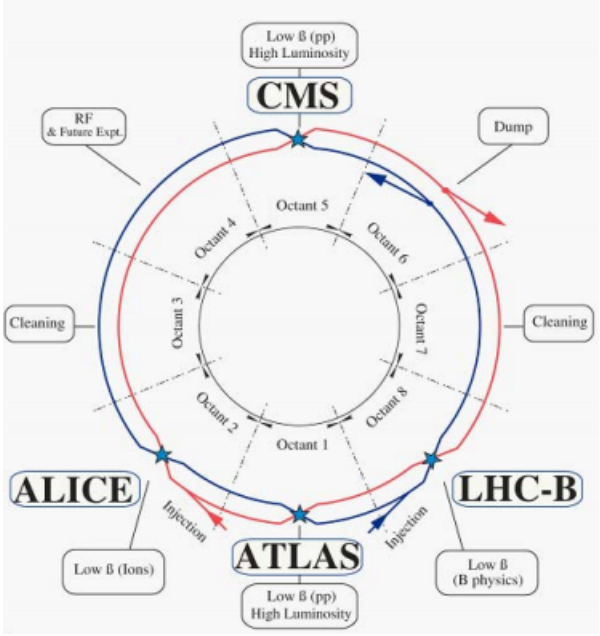

Figure 9: Schematic layout of the LHC. [11]

In addition to these four experiments, there are two small detectors designed to measure scattering at very small angles, with the main purpose of determining the proton-proton total cross sections, they are TOTEM which is installed around Point 5 and LHCf which is installed around Point 1.

ATLAS and CMS are both multi-purpose experiments whose main physics goals are: the search for the Higgs boson, and exploration of any possible new physics in the energy ranges provided by the LHC.

The instantaneous luminosity given by the accelerator is different at each of these experiments, it has a maximum at CMS and ATLAS with a designed optimal value of $L = 10^{34} cm^{-2} s^{-1}$. This value has not been reached yet. The total integrated luminosities during 2010, 2011 and 2012 Runs in CMS are shown in figure 10.

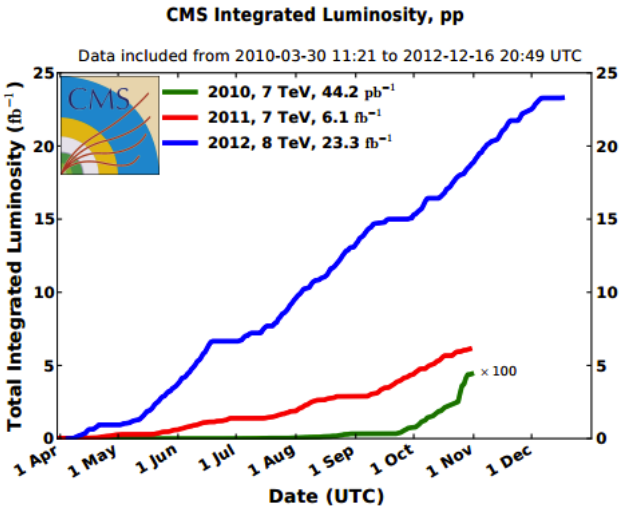

Figure 10: Integrated Luminosity in CMS as function of time. [12]

To reach the described performance, the LHC uses superconductive magnets. These magnets work at 1.9 K, which is the lowest temperature of any superconducting accelerator to date. The main dipoles of the LHC can produce a magnetic field of 8.4 Tesla at a current of 11700 A approximately. Each one of these magnets has a length of 14.3 m. The entire accelerator has 1232 of these dipoles.

2.1 The CMS Detector

The CMS (Compact Muon Solenoid) Detector is installed in Point 5 of the LHC. This point is located at Cessy, France on the north side of the LHC ring, as can be seen in figure 9.

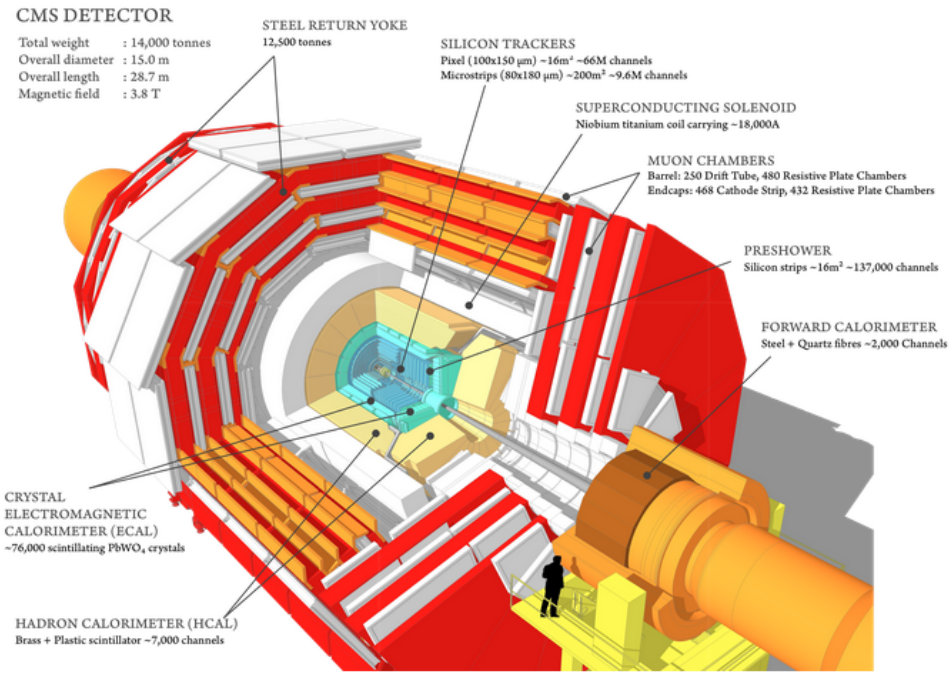

Figure 11: Sectional view of the CMS detector. [13]

The CMS is a general purpose particle detector. It has a cylindrical shape with a length of 21.6 m and a diameter of 14.6 m. It is installed inside a cavern that is located 100 m underground. Its mechanical structure is defined by the large Iron yoke that is used to collect the magnetic field that comes out of the central solenoid. This yoke gives CMS a cylindrical shape. The yoke is segmented into 5 "wheels" that define the Central Barrel and three rings of each side of the barrel that defined two "end-caps". Inside this yoke there is a central region delimited by Large superconducting solenoid. Inside the solenoid there is a silicon tracker, an electromagnetic calorimeter (ECAL) and a hadron calorimeter (HCAL). Outside the magnet, and inserted in the yoke structure are the muon detectors, composed of layers of Drift Tubes (DT) and Resistive Plate Chambers (RPC) in the barrel and Cathode Strip Chambers (CSC) and RPCs in the end-caps. The geometrical structure of the CMS Detector systems can be seen on figure 11.

Due to its large iron yoke the CMS Detector is very heavy (14 Kt). It is also compact in comparison with similar detectors since it does not require an external magnetic field for the muon system. This is because the iron of the massive yoke compactified the magnetic field coming out the solenoid, making it intense enough to deflect the muons. It is optimized to detect and trigger on muons. The central magnet is a very large superconductive solenoid of 13 m long and 6 m in diameter, that provides an inner magnetic field up to 3.8 T, and outer magnetic field of the order of 2 T (for the muon tracking system).

2.1.1 The Tracker System

In inner most part of the CMS Detector, surrounding the interaction point, a high resolution silicon tracker is located. This tracker has also a cylindrical shape with the length of 5.8 m and a diameter of 2.5 m.

The tracker is composed of an inner pixel detector and the silicon strip detectors (SSD) surrounding it. This system is designed to reconstruct the tracks of charged particles coming out of the interaction point with the highest space resolution. Due to its location near the beam pipe, the silicon tracker must support high doses of radiation.

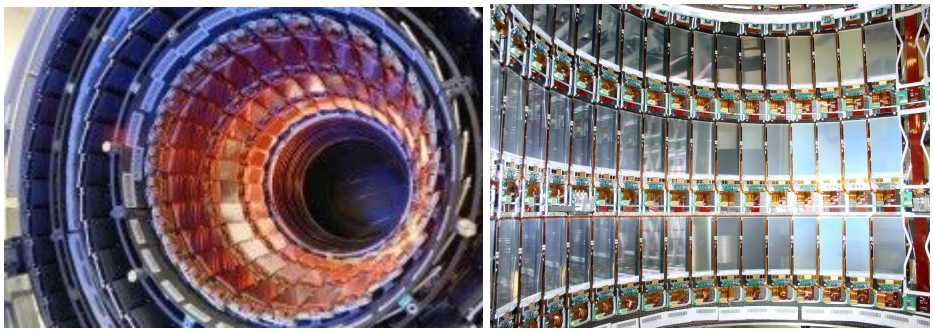

Figure 12: (Left) Picture of the CMS Tracker showing silicon strips detectors in the barrel module. (Right) Picture of the inside inside of the Tracker Inner Barrel Layer 3. Each panel in both pictures is compose by several silicon strips. [14]

The LHC was designed to reach a luminosity of $10^{34} cm^{-2} s^{-1}$. With the very high luminosities of the LHC, around of 1000 particles will pass through the tracker every 25 ns. This requires a very fast response to correctly reconstruct tracks and give them the correct timing information.

Due to its proximity to the interaction point the tracker is very important for detecting short-lived particles, that would not leave direct signal in the detectors, but would be reconstructed from their decay products. The resolution with which the tracks of the decay products are measured will determine if the original state can or cannot been reconstructed and the accuracy with which it is done. This is the crucial role for the silicon tracker since most of the interesting states are very short-lived and its reconstruction is very important (For example the reconstruction of the b-quarks out of b-jets).

2.1.2 Electromagnetic Calorimeter ECAL

The second sub-detector coming out of the interaction point is the Electromagnetic Calorimeter (ECAL). It is a homogeneous and hermetic calorimeter made out of 61200 lead tungstate crystals ($PbWO_4$) in the barrel and 7324 crystals in each of the two end-caps. This material was chosen because it is a scintillator crystal with short radiation length that has high radiation endurance. The lead tungstate is highly transparent and scintillates when electrons and photons pass through it. The properties of this material allows for a compact calorimeter with high granularity and fast response. The light produced by the crystals is collected and transduced by photodiodes in the barrel and vacuum photo-triodes in the end-cap.

Additional detectors, called pre-shower detectors, are placed in front of the two end-caps; they are used to increase the resolution in the forward regions with the purpose of identifying neutral pions decaying into two photons in that angular region. The pre-shower system has two layers: lead radiators initiate electromagnetic showers from incoming photons/electrons, while silicon strip sensors measure the deposited energy and the transverse shower profiles.

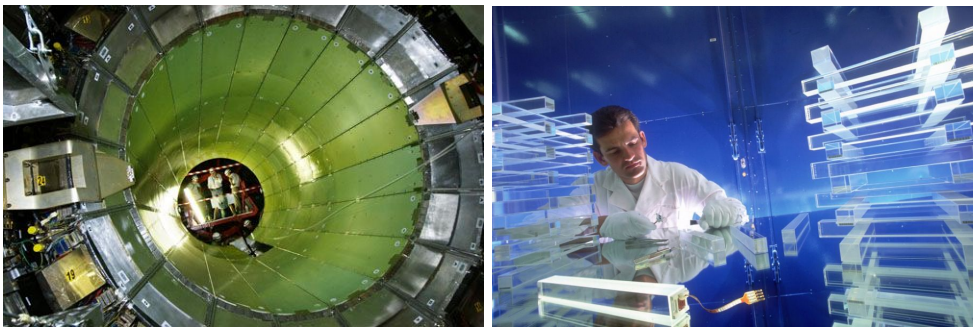

Figure 13: (Left) CMS ECAL during construction. (Right) Lead tungstate crystals for the CMS ECAL [15].

2.1.3 Hadronic Calorimeter HCAL

The third sub-detector coming out of the interaction point is the Hadronic Calorimeter (HCAL), designed to measure the energy of hadrons produced as a result of the collisions. Additionally, the HCAL provides indirect measurement of the presence of non-interacting neutral particles, such a neutrinos or other unknown particles with this feature. This is done through the measurement of the energy balance of the collision in search for large amounts of missing transverse energy.

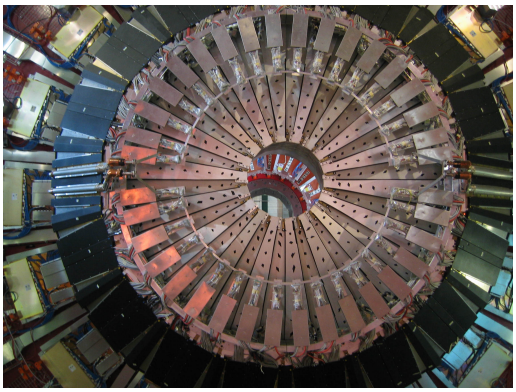

Figure 14: View of a CMS HCAL Endcap.

The HCAL is composed of plastic scintillator tiles with wave length shifting (WLS) fiber readout embedded. Tiles are interleaved with stainless steel and copper layers. The metal layers absorb hadrons and the plastic scintillator regions detect the particles that cross them. The HCAL plays an important roll when triggering events due to missing energy, like the one produce by SUSY particles like neutralino, for example.

The hadron calorimeter Barrel and end-caps surround the tracker and ECAL, as seen from the interaction point. The HCAL Barrel is surrounded in term by the superconducting solenoid. This design constraints the total amount of material used to develop and absorb the hadronic showers, therefore a small HCAL is placed outside the solenoid to detect any energy that might have leaked out of the HCAL and the solenoid.

CMS has two separate forward calorimeters (HF), located at 10.9 m in each side, from the interaction point. These calorimeters use quartz fibers as active material, embedded in copper.

2.1.4 Muon System

The muon system is located outside the solenoid magnet, it is composed of chambers inserted inside the yoke wheels in the barrel and between the yoke disks in the end-caps (see figure 15).

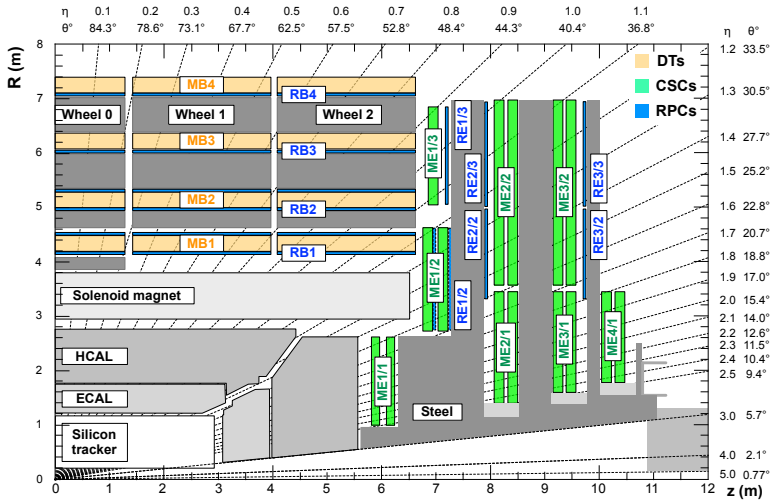

Figure 15: Barrel and endcap muon chamber in CMS. [16]

The detection of muons is very important for CMS. The presence of muons in an event might indicate interesting signatures, specially for analyses searching for topologies involving high pT particles. There is a dedicated trigger system (see 2.1.5) on CMS to select events containing muons. The muon system therefore was designed to respond very fast in order to provide the trigger and to reconstruct the tracks with high momentum resolution. Good muon momentum resolution and trigger capability are enabled by the high-field solenoidal magnet and its flux-return yoke. The yoke serves as a hadron absorber cleaning up the muon signal and providing curvature for the track outside the solenoid.

The muon system is the result of the use of three different detector technologies: Drift Tubes (DT), Resistive Plate Chambers (RPC), and Cathode Strip Chambers (CSC). DTs and CSCs are optimized tracker detectors while the RPCs are optimized trigger detectors that also provide redundant tracking information. The DTs are located in the Barrel region, the CSCs are located in the end-caps, and the RPCs are located in both, barrel and end-caps. The DTs and CSCs have high space resolution while the RPCs have high time resolution.

The Drift Tubes (DT)

The DTs are used for triggering and tracking on muons. The DTs are aluminum cells with a thickness of a few inches. These cells are filled with gas and have an anode wire in the center. The anode wire collects electrons resulting from the charged particles passing through the gas. These cells are ensembled in units called chambers, with four layers of cells each. These layers have different orientations in order to provided 2D information, as well as timing information. From this signal plus drift time information two coordinates can be measured for every detected particle: the position in the wire where the electrons hit, and the distance that those electrons traveled before hitting the wire.

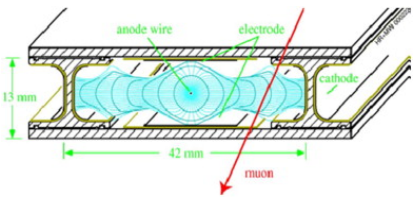

Figure 16: The drift tube cell of CMS [16]

A chamber contains three super-layers, the super-layers are groups of four layers of drift cells. There are four levels of DT chambers moving radially out of the interaction point. These DT chambers are complemented by RPC chambers, in what is called a "muon station" , therefore there are four levels of muon stations in the barrel. These stations are segmented in azimuth angle into twelve sectors (forming a dodecagonal structure). Along the z-axis there are five wheels. Therefore in terms of muon stations one has four levels radially, 12 sectors azimuthally and 5 wheels along the z-axis.

The Cathode Strip Chamber (CSC)

The CSCs are designed to trigger on and reconstruct the tracks of muons in the end-caps, where the magnetic field is not uniform, therefore a detector with a good space resolution in two dimension like a CSC is needed. This type of detector consist of positively charged anodes wires and negatively charged cathode strips made out of copper, orientated at 90 degrees respect to the wires. This grid is located inside a chamber filled with ionizing gas. When a muon passes through a CSC chamber, it knocks out electrons from the atoms of the gas. These electrons drift until they reach the anode wires, leaving behind positive ions that move to the copper strips. This process creates two currents that can be registered, giving the CSC a very good spatial resolution in two dimensions.

Figure 17: Cathode Strip Chambers mounted on a CMS endcap. [16]

The CSC system in each end-cap is composed by four disks of chambers mounted on a metallic structure.The inner disk has three rings of chambers, while the other three disks are composed by two rings of chambers. In each ring there are 18 chambers, with the exception of the outer ring which has 36 chambers. There are 468 chambers in total, located in modules that contain six layers of chambers each. This arrangement allows for accurate identification of muon tracks, and a match with tracks reported by the inner tracker.

The Resistive Plate Chambers (RPC)

The RPCs are used both in the barrel and in the end-caps, providing redundant information for triggering and tracking in both regions. These are gaseous parallel plate cameras that combine adequate spatial resolution with excellent temporal resolution ($\sim$1 ns). The temporal resolution and fast response of RPCs make them very important in the trigger system because they identify the correct bunch crossing associated with the detected track. The two plates are separated few millimeters, creating a gap in which the gas is located. This gas is ionized by the particles when they pass through it; the ionization produced generates an electron avalanche that will induce a signal in metal strips located on the outside of the plates.

A total of six layers of RPCs are embedded in the barrel iron yoke. Each layer of RPC forms a dodecagon with full 2π azimuth coverage. Two layers are located in each of the first two muon stations, and one in each of the

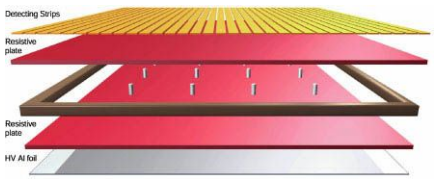

Figure 18: Resistive Plate Chamber layers. [17]

two last muon stations. The end-caps are instrumented with four layers of RPCs, corresponding to four disks. In each disk there are three rings of RPCs.

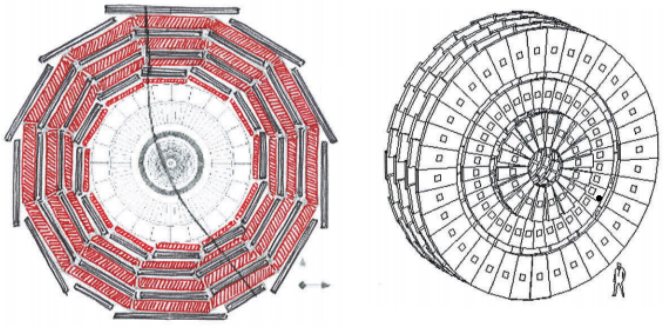

Figure 19: (right) Barrel design of a muon system in CMS . (left) Perspective view of the CMS Endcap muon chamber layout. [17]

2.1.5 Trigger and DQM System

The CMS sub-detectors sum up about 100 millions of electronic readout channels, which provide information about the results of the p-p collisions every 25 ns (at the highest design luminosity). This amount of data cannot be recorded. Also most of these interactions are not interesting for physics studies; therefore the data must be filtered quickly by a system that selects automatically only the interesting events, the CMS Trigger System.

The trigger system reduces the rate of collisions and selects only the events that seem interesting. This is done in two levels: a Level-1 trigger (L1) that quickly selects events based on the presence of muon-like tracks and high energy depositions in the calorimeters, and a High Level Trigger (HLT) that uses more elaborated software algorithms to search for signature of different kinds of interesting physics.

Level-1 Trigger

The fist step of the CMS Trigger, the L1 Trigger, is executed by very fast electronics. This electronics selects events that match with physical patterns that suggest high P_T physics. The L1 trigger reduces the amount of data from about one billion to about one hundred thousands interactions per second.

The L1 system must readout the signal, make a decision, and send the accepted events to a buffer for the HLT in approximately $3.2\mu s$. Every operation in the L1 should be repeated every 25 ns. The L1 is divided in three subsystems: L1 Global Calorimeter Trigger, L1 Global Muon Trigger and L1 Global Trigger.

High Level Trigger (HLT)

The goal of the High Level Trigger is to select interesting physics candidates, doing a more sophisticated reconstruction and selection on the events that passed the L1 trigger, reducing the trigger rate from about one hundred thousand to only about one hundred events per second. The HLT trigger is implemented in software and run in a farm of a thousand very fast CPUs, where simplified reconstruction algorithms are executed. The criteria of the HLT algorithms are more sophisticated than the ones used by the L1 trigger. The reconstruction of the objects in the HLT should be as close as possible to the off-line reconstruction. At the HLT level several algorithms running in parallel in order to search for signatures of different kinds of interesting physics, putting a "tag" on the events that pass the pre-established criteria. Once the HLT has accepted events, it splits them into datasets depending on the triggers path they followed, and send them to hard disks.

2.2 Higgs Physics in CMS

In July 2012, CMS and ATLAS announced the discovery of a new particle consistent with the predictions of the standard model (SM) for the Higgs boson. The first research of the Higgs boson search have come from five decay channels: H→ $\gamma\gamma$, ZZ, W^+W^-, $\tau^+\tau^-$ and $b\bar{b}$ which, according to the SM have the most significant branching ratios. Recent results presented at the Moriond conference 2013 take into account about 5 fb^{-1} of data at 7 TeV and 20 fb^{-1} at 8 TeV.

2.2.1 $H \to \gamma\gamma$

The $H \to \gamma\gamma$ decay channel provides a clean final state with a mass peak at $m_H \sim 125.3 \pm 0.6$, that can be reconstructed with high precision. $H \to \gamma\gamma$ was the most important channel in the initial search of the Higgs. At the Higgs mass $m_H \sim 125.3$ GeV, the branching ratio is around 0.21%. The search in this channel was made looking for a narrow peak in the diphoton invariant mass on a large irreducible background coming out of QCD process in the two photon production. The analysis used multivariate techniques for the selection and classification of the events. The dataset used for the analysis consists of events with diphoton triggers. Also, diphoton triggers with asymmetric transverse energy, E_T, as well as other complementary photon selections criteria, were used.

Photon candidates were reconstructed from clusters of ECAL channels around significant energy deposits. Jets, used in the dijet tagging, were reconstructed using particle-flow, which uses the information of all sub-detectors of CMS to reconstruct each particle track. The reconstruction of the primary vertex of the diphoton candidate was performed using the kinematic properties of all the tracks associated with this vertex and their correlations with the diphoton kinematics.

The event selection required two photon candidates that satisfy p_T requirements and a "loose" photon identification criteria [18]. These photons must be reconstructed into the region $|\eta| < 2.5$, excluding the barrel-endcap transition region $1.44 < |\eta| < 1.57$. The excluded barrel-endcap transition region removes from the acceptance the last two rings of ECAL crystals in the barrel and the first ring of trigger towers in the end-caps. A p_T threshold of $m_{\gamma\gamma}/3$ was applied to the leading photon and $m_{\gamma\gamma}/4$ to the sub-leading photon. In the case of events passing the dijet selection, the requirement for the leading photon is $m_{\gamma\gamma}/2$.

The dominant background to $H \to \gamma\gamma$ consists of the irreducible background from the prompt diphoton production and from $pp \to \gamma + jet$ and $pp \to jet + jet$, where one or more photons is not a prompt photon. Isolation is a powerful tool to reject the non-prompt background due electromagnetic showers originating in jets. In addition to isolation criteria the following variables were also taken into account: the ratio between hadronic energy behind the photon and the photon energy, the transverse width of the electromagnetic shower and an electron track veto. Photon candidates in the barrel have less background than those in the end-caps, for this reason it is useful to divide photon candidates into four categories and apply a different selection on each of them.

Events in which a Higgs boson is produced by VBF have two forward jets. Jet selection criteria are applied to the two jets of largest p_T in events within $|\eta| < 4.7$. The p_T threshold of the two jets is 30 and 20 GeV, their

separation in η should be greater than 3.5. The dijet invariant mass must be greater than 350 and 250 GeV for data with $\sqrt{s} = 7$ and $\sqrt{s} = 8$ TeV respectively. Two additional selection criteria over the dijet are applied: the difference between the average pseudo-rapidity of the two jets and the pseudo-rapidity on the diphoton must be less than 2.5, and the difference in azimuthal angle between the diphoton and dijet must be greater than 2.6 radians.

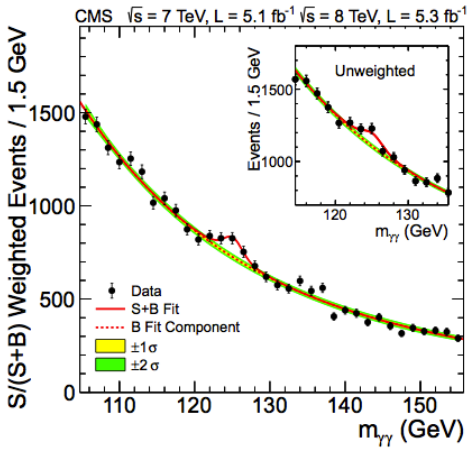

Figure 20: The diphoton invariant mass distribution [1]

Figure 20 shows the results of CMS data for this channel. The signal model, and the background model, are all weighted; the weights are normalized such that the integral of the weighted signal mode matched the number of signal events given by the best fit. The excess of events around 125 GeV is evident in the distribution, and agree pretty well with the Higgs boson of the SM.

2.2.2 $H \to ZZ$

The studies of the decay channel $H \to ZZ \to 4l$, where $l = e,\mu$, are crucial to the determination of some properties like the spin and the parity of the discovered boson. The SM predicts that the Higgs boson should have zero spin and positive parity (represented as $0+$), the zero-spin can be checked through the lack of the polar (and azimuthal) angle correlations between the initial state and final state particles in the combined process of production $gg \to H$ and decay $H \to ZZ$. [19]

The most recent results (Moriond 2013) for the $H \to ZZ \to 4l$ channel used 5.1 fb^{-1} of CMS data collected at $\sqrt{s} = 7$ TeV, and 19.6 fb^{-1} collected at $\sqrt{s} = 8$ TeV, corresponding to the whole dataset available. Additionally, a comprehensive search for other SM-like Higgs boson particles was also performed looking at the the $H \to ZZ \to 4l$ and $H \to ZZ \to \tau^+\tau^-$ channels.

The events that are used by the analysis, are selected by the trigger system that requires the presence of a pair of electrons or a pair of muons, or a triplet of electrons. Also, triggers where an electron and a muon appear were used. The momentum requirement is a minimum of 17 GeV for the first lepton and 8 GeV for the second one, in the case of double lepton triggers. For the triple electron trigger, the minimum momenta are 15, 8 and 5 GeV, respectively. Monte Carlo (MC) samples were used to optimized the event selection and to evaluate the acceptance and systematic uncertainties.

The event selection include the signals for both channels, $H \to ZZ \to 4l$ and $H \to ZZ \to 2l2\tau$. The selection for the candidates in the $4l$ analysis uses isolated and well identified primary leptons. The lepton isolation requires that the Z+jet, $Zb\bar{b}$ and $t\bar{t}$ background be suppressed. The photon associated with the closest lepton, and which makes the "dressed" lepton-pair mass closer to the Z mass, are kept in the building of Z candidates. The candidate events are required to have two pairs of leptons, each pair is composed of same flavor and

opposite charge particles (l^+l^-). The pair with an invariant mass closest to the nominal Z mass is denoted m_{Z_1} and it must satisfy $40 < m_{Z_1} < 120$ GeV. All remaining leptons are considered and a second pair of leptons, with mass denoted m_{Z_2} must satisfy: $12 < m_{Z_2} < 120$ GeV. If more than one Z_2 candidate satisfies all criteria, the ambiguity is resolved by choosing the pair of leptons with the highest scalar sum of p_T . Among the four selected leptons forming Z_1 and Z_2, at least one must have $p_T > 20$ GeV and the other one $p_T > 10$ GeV [20].

For the $2l2\tau$ final state, events are require do have $Z_1 \to l^+l^-$ with one lepton at $p_T > 20$ GeV and the other one at $p_T > 10$ GeV, and $Z_2 \to \tau^+\tau^-$ with τ decaying into μ, e and τ_h. The invariant mass of the reconstructed Z_1 is required to satisfy $60 < m_{ll} < 120$ GeV, and Z_2 must satisfy $m_{min} < m_{\tau\tau} < 90$ GeV, where $m_{min} = 20$ GeV for $Z_2 \to \tau\tau \to e\mu$ final states, and 30 GeV for all others.

In the $H \to ZZ \to 4l$ decay mode a search was made for a narrow four-lepton mass peak in the presence of a small continuum background. Since there are differences in the irreducible background rates and mass resolutions between sub-channels $4e$, 4μ and $2e2\mu$, they are analyzed separately. The background sources include an irreducible four-lepton contribution from direct ZZ production via $q\bar{q}$ and gluon-gluon process. Reducible contributions come from $Z + b\bar{b}$ and $t\bar{t}$ production where the final states contain two isolated leptons and two b-quark jets producing secondary leptons. Additional background arises from Z+jets and WZ+jets events where jets are misidentified as leptons.

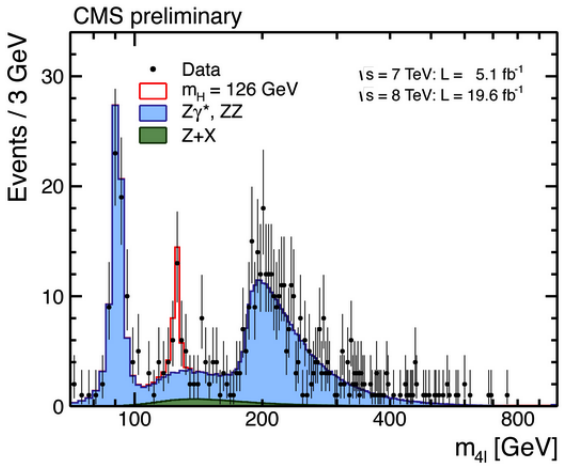

Figure 21: Distribution of the four-lepton reconstructed mass in the full mass range for the sum of $4e$, 4μ and $2e2\mu$ channels [20].

Figure 21 shows the reconstructed four-lepton invariant mass for the $4l$ channel combining $4e$, 4μ and $2e2\mu$ data. A very clear peak around 126 GeV is seen, confirming the results of July 2012. The new boson discovered by CMS and ATLAS experiments is observed in the $4l$ channel, with a local significance of 6.7σ.

2.2.3 $H \to W^+W^-$

Another decay channel studied by CMS is the $H \to W^+W^-$. The final state of this decay is $2l2\nu$, where l is a charged lepton, electron or muon, and ν a neutrino. In the latest results presented at Moriond 2013 the event sample corresponded to the full integrated luminosity collected by CMS in 2011 and 2012. This channel was analyzed by selecting events in which both W bosons decay leptonically, resulting in a signature with two isolated, oppositely charged, high p_T leptons (electrons or muons) and large missing transverse energy (E_T^{miss}), due to the undetected neutrinos. To improve the sensitivity of the signal, the events were separated according to the lepton flavor and jet multiplicity, into the samples: e^+e^-, $\mu^+\mu^-$, $e^\pm\mu^\mp$, 0-jet and 1-jet. Events with more than one jet were rejected.

The events were selected by triggers which require the presence of one or two high-p_T electrons or muons. Two opposite charged candidates are required, with $p_T > 20$ GeV for the leading lepton and $p_T > 10$ GeV for the trailing lepton. For the 2011 data, at $\sqrt{s} = 7$ TeV, the trailing lepton p_T threshold is 15 GeV for e^+e^- and $\mu^+\mu^-$. Only electrons with $|\eta| < 2.5$ were considered. For the muons, the criteria was $|\eta| < 2.4$ [21].

Muons were required to be isolated to distinguish those resulting from W-boson decays and those resulting from QCD background process, which are usually present within or near jets. Electron candidates were identified using a multivariate approach, which obtains information from the tracker and the ECAL. The lepton candidates where required to originate from the primary vertex of the event. Additionally, significant amount of missing transverse momentum should be present, since this fixture is associated with the signal events but not present in the background events.

For this channel, the main backgrounds are irreducible resonant WW production and reducible W+jets process. To suppress the top quark background, a top-tagging technique, was used. In this technique events with soft-muons are rejected since they come from semi-leptonic b-decays, that come from top-quark decays. B-jet tagging is also used in order to reject background from WZ. Any event that has a third lepton that passes the identification criteria is also rejected.

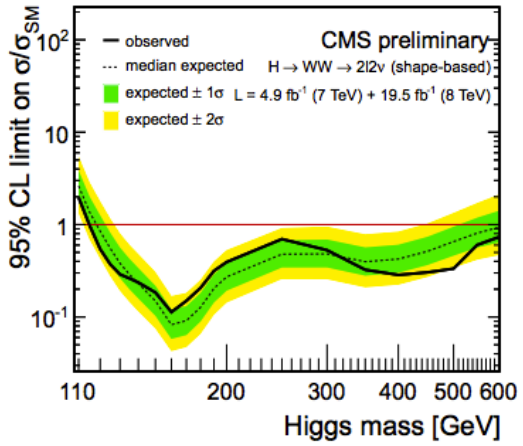

Figure 22: Expected and observed 95% upper limits on the cross section times branching fraction for $H \to W^+W^-$ channel, relative to the SM Higgs expectation for shape-based analysis using the 7+8 TeV data [21].

An excess of events was observed in the "low Higgs boson" mass. Due to the poor mass resolution over this channel the excess extends over a large mass range. Figure 22 shows the expected and observed 95% CL on the cross section times branching fraction for this channel. A Higgs with $m_H = 125$ GeV has been added to the background processes. The significance of the excess with respect to the background at 125 GeV are 2.2 and 3.5 σ for the 7 and 8 TeV , respectively, and 4.0 σ for the 7+8 TeV combination.

2.2.4 $H \to \tau^+\tau^-$

According to the spontaneous symmetry breaking of the SM, the Higgs not only couples to bosons but also to fermions (quarks or leptons). An important test of whether the discovered boson is indeed the SM Higgs or not is to observe its decay into fermions. CMS performed a search for the decay of the new boson into τ leptons. When the discovery announcement was made in July 2012, the observations in this channel were not conclusive. Since then, with the additional data recorded by CMS, a clear signal in this channel has emerged for a boson with a mass of around 125 GeV.

The decay mode $H \to \tau^+\tau^-$ was studied for five independent final states: $\mu\tau_h$, $e\tau_h$, $e\mu$, $\tau_h\tau_h$ and $\mu\mu$, where τ_h is a reconstructed hadronic τ decay. In each channel, the signal was separated from the background, and

particularly from the irreducible $Z \to \tau\tau$, using the τ-pair mass $m_{\tau\tau}$ reconstructed from the four-momenta of the visible decay products of the two τ leptons and from the E_T^{miss}. Events were classified according to additional jets in the final state: the 0-jet constrain the background normalization, identification efficiencies and energy scales. The 1-jet selects signal events with a Higgs boson produced by gluon-fusion or in association with W or Z bosons decaying hadronically.

The trigger selection required a combination of electron, muon and tau trigger objects. In the fully hadronic $\tau_h\tau_h$ final state two τ_h objects with $p_T > 30$ GeV were required, together with a jet trigger object with $p_T > 30$ GeV and $|\eta| < 3.1$ [22]. For the $e\tau_h$ and $\mu\tau_h$ final states the events were selected containing an electron of $p_T > 20$ GeV or a muon with $p_T > 17$ GeV, located within $|\eta| < 2.3$. In the $e\mu$ final state events were selected with an electron with $|\eta| < 2.3$ and an oppositely charged muon with $|\eta| < 2.1$, requiring $p_T > 20$ GeV for the leading lepton and $p_T > 10$ GeV for the sub-leading lepton. In the $\tau_h\tau_h$ final state, both τ_h objects were required to have $p_T > 45$ GeV and $|\eta| < 2.1$ [23].

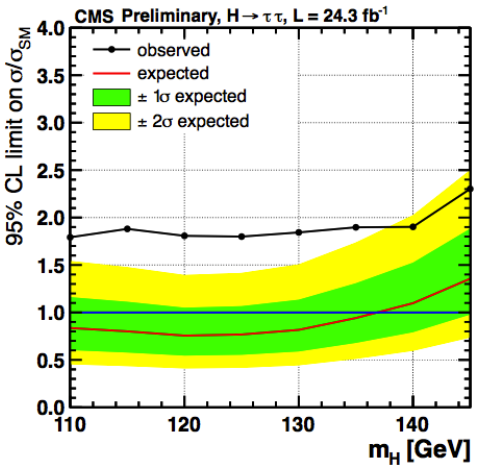

Figure 23: Observed 95% upper limit on the $H \to \tau^+\tau^-$ signal, together with the expected limit obtained in the background hypothesis. The bands show the expected one and two σ probability intervals around the expected limit. [23].

In the $e\tau_h$ and $\mu\tau_h$ final states, events with more than one loosely identified electron or muon with $p_T > 10$ GeV were rejected to reduce the $Z \to ll$ background. The overlap between the various channels is eliminated by rejecting in each channel events with an additional lepton. In the $\mu\mu$ final state the sample of dimuon events is largely dominated by the $Z \to \mu\mu$ background, this background is suppressed combining the follow variables: the ratio of the p_T of the dimuon system to the scalar sum of the two muons p_T, the significance of the distance of closest approach between two muons and the η of the dimuon system.

Figure 23 shows the observed 95% CL upper limit obtained, together with the expected limit obtained in the background hypothesis for the combination of the all $\tau\tau$ channels. An excess is visible in the observed limit with respect to the limit expect for the background hypothesis. Figure also shows the observed and expected limits obtained in the signal plus background hypothesis.

2.2.5 $H \to b\bar{b}$

For the $H \to b\bar{b}$ channel, the studies were focused on Higgs bosons produced in association with at least one b quark. The latest results, presented in Moriond 2013 used 2.7- 4.8 fb^{-1} of CMS data collected at 7 TeV. The analysis used events passing a jet-trigger, with at least 3 jets candidates identified (tagged) as coming from the b-quark (b-jets). A signal would be identified as a peak in the invariant mass distribution of the two leading b-jets. Events in the data with only two b-tags among the three leading jets are used to model the background.

Events are accepted if two or three of the b-jets are produced with $|\eta| < 2.6$. Data selection was divided into three categories according to the triggers used. The first category is caracterized by dijet triggers with $p_T < 46$ GeV and the next-to-the-leading jet with the $p_T > 38$ GeV. The second category requires dijet triggers with $p_T > 60$ GeV and the next-to-the- leading dijet triggers with $p_T > 53$ GeV. The third category is similar to the first but requires a third jet with $p_T > 20$ GeV [24].

The dominant background comes from QCD multijet production with two or more jets containing b hadrons, and can not be fully reduced by kinematic selection. For this reason a method based on control data samples was applied.

In the semileptonic final state, a signal is searched in events with three identified b-jets and an additional non-isolated muon. A peak in the invariant mass distribution of the two leading jets is demanded. The muon requirement reduces the absolute signal efficiency, since it selects events where at least one of the b quarks decayed semileptonically thought a muon. To reduce the event rate at the trigger level a lower threshold for the jets, was allowed.

The data used in the semileptonic analysis was collected using different trigger selections, depending on the luminosity. All the triggers required a muon with a $p_T > 12$ GeV and the presence of one or two central jets ($|\eta| < 2.6$) with $p_T > 20$ or 30 GeV. As in the all-hadronic final state, the major backgrounds for the semileptonic case are multijet events from hard-scattering processes. Other possible backgrounds from events with multiple vector bosons like ZZ, ZW, WW are negligible. For this channel, signal has not yet been observed above the SM background expectations.

2.2.6 $H \to Z\gamma$

Among the Higgs couplings, the $H \to Z\gamma$ is interesting in many aspects, for instance, the interaction of the Higgs with the photons does not occur at tree-level because the photon is massless. The $H \to Z\gamma$ coupling is induced by loops of charged particles, dominated by the heaviest ones, like the W boson and the top quark (see figure 24).

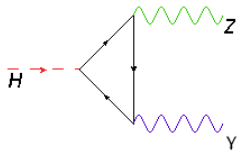

Figure 24: Feynman diagram for the Higgs decay into a Z boson and a photon.

Due to the presence of the loop of charged particles which are massive, the channel is very sensitive to physics beyond the standard model since new particles that are very massive and charged, could contribute, resulting in a different branching fraction from the one predicted by the SM. Despite the small value of this branching fraction, which in the SM varies between 0.111% and 0.246%, the CMS experiment will be sensitive to this channel in the near future. Additionally, since there is no missing energy, this channel has a good mass resolution, and the only relevant background is due to the proton-proton to diboson process.

The most recent CMS analysis of this channel (Moriond 2013) uses data samples corresponding to an integrated luminosity of 5.0 and 19.6 fb^{-1} of data recorded by CMS during 2011 and 2012. The basic selection requires events with two opposite-sign, same-flavor leptons (e or μ) consistent with a Z-boson decay and a photon: $e^+e^-\gamma$, $\mu^+\mu^-\gamma$. All particles must be isolated and have $p_T > 20$ GeV for the leading lepton, $p_T > 10$ GeV for the trailing lepton and $p_T > 15$ GeV for the photon. The electrons and the photon must have $|\eta| < 2.5$, and the muons $|\eta| < 2.4$. Electrons and photons in the barrel-endcap transition region, that correspond to $1.44 < |\eta| < 1.56$ are excluded. The invariant mass of at least one l^+l^- pair is required to be greater than 50 GeV. The dominant background to $H \to Z\gamma$ comes from the production of Z accompanied by γ, and the reducible backgrounds from final state radiation in Z decays and Z+jets, where a jet or a lepton is misidentified

as a photon.

Events are required to have at least one good primary vertex, with the reconstructed longitudinal position within 24 cm of the geometric center of the detector and the transverse position within 2 cm of the beam interaction region. In the case of multiple vertices, the one with the highest scalar sum of the p_T^2 of its associated tracks is chosen. All leptons which are used to select events, must come from the same primary vertex.

Photon candidates are reconstructed from clusters of channels in the electromagnetic calorimeter with significant energy deposits. In the endcaps, in the regions where the preshower detector is present ($|\eta| > 1.65$) the energy deposits in this detector are added. The observables used in the photon selection are: isolation variables based on the particle flow algorithm, the ratio of hadronic to electromagnetic energy deposited in the calorimeter system, and the transverse width of the electromagnetic shower. Also an electron veto is imposed in order to avoid misidentifying electrons as photons.

The electron reconstruction starts from clusters of energy deposited in the electromagnetic calorimeter, which are matched to hits in the silicon tracker. Electrons are identified using variables which include the ratio between the energy deposited in the hadron and the electromagnetic calorimeters, the shower width in η and the distance between the calorimeter shower and the particle trajectory in the tracker, measured in both η and ϕ.

Muon candidates are reconstructed with a global fit to the tracks recorded by the tracker and the muon system ("Global Muons"). A high quality is demanded in the global fit to the track trajectory.

The sensitivity of the event selection can be enhanced by subdividing the events into classes according to indicators of the expected mass resolution and the signal to background ratio. Four mutually exclusive event classes are defined in terms of the pseudo-rapidity of the leptons and the photon, on the shower shape of the photon, and the R_9 value of the photon for events with the two leptons in the barrel. The R_9 variable is defined as the energy sum of groups of 3×3 crystals centered on the crystal with the highest energy deposition in the supercluster, divided by the energy of the supercluster. The event classes are defined as follows: event classes 1 and 2 have the leptons and the photon in the barrel, class one has the events with high R_9 and class two has low R_9; event class 3 has at least one lepton in the endcap and the photon in the barrel; finally, event class 4 has the leptons and the photon in the endcaps. The background model is obtained by using different polynomial fits to the $ll\gamma$ mass distribution for the different event classes [25].

The systematic uncertainties come mostly from the measurement of the luminosity, the trigger efficiency, the uncertainty in the Higgs branching fraction prediction, the corrections applied to the simulation to reproduce the performance of the lepton and photon selections, the event migration caused by the requirements on the photon shape in the event classification, and the signal modeling. Based on the fit-bias studies, the uncertainty on the background estimation due to the chosen functional form is estimated to be negligible.
After performing this analysis on the data samples at 7 and 8 TeV, recorded in 2011 and 2012, no statistical evidence of a Higgs boson is observed in this channel, and therefore the data is used to derive upper limits for cross section. The expected exclusion limits at 95% CL are between 6 and 19 times larger to the SM cross section prediction and the observed limit fluctuates between about 3 and 31 times this value. Both limits are shown in the figure 25.

In summary, up to the results presented in Moriond 2013, using data collected by CMS in 2011 and 2012, an excess of events was observed above the expected background, with a local significance of 5.0 standard deviations at a mass near 125 GeV. The studies were made principally in the six channels mentioned above. The excess is most significant in the two decay modes with the best mass resolution: $\gamma\gamma$ and ZZ. In the next section, the Higgs Dalitz decay channel will be presented in detail since it is the subject of my PhD dissertation.

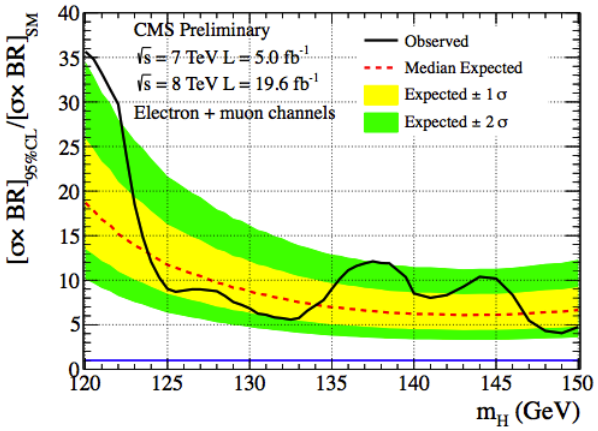

Figure 25: Expected and observed exclusion limit on the cross section of a SM Higgs boson decaying into Z-boson and a photon as a function of the boson mass based on 5.0 fb^{-1} at of data taken at 7 TeV and 19.6 fb^{-1} at 8 TeV.

3 The Dalitz Decay $H \to \gamma\gamma* \to \gamma l^+ l^-$

The subject of my PhD dissertation is the study of the Dalitz decay of the Higgs boson using the CMS detector and the data collected in proton-proton collisions at 8 TeV. This decay could be seen as a QED radiative correction of the $H \to \gamma\gamma$ decay channel in which one of the γ becomes in dilepton. Due to the different nature of the detection of a gamma as compared to the detection of charged leptons, the Dalitz decay becomes a different problem from the experimental point of view, being closer to $H \to \gamma Z \to \gamma l^+ l^-$. The name "Dalitz decay" comes from one of the decay channels of the neutral pion : $\pi^0 \to \gamma e^- e^+$. This decay is actually the result of the dominant decay $\pi^0 \to \gamma\gamma$ in which one of the γ is virtual (γ^*) and then becomes an electron-positron pair due to a QED process. A similar situation can happen to the $H \to \gamma\gamma$ decay channel, where one of the γ is virtual and then becomes a dilepton. Since the Higgs is much more massive than the π^0 one can have muon, electron or tau dileptons. The complex nature of the tau decay makes the τ-dilepton case a completely different experimental problem, therefore in this work we will focus on the electron and muon dileptons. Figure 26, shows a Feynman diagram illustrating how the Dalitz decay proceeds in this case.

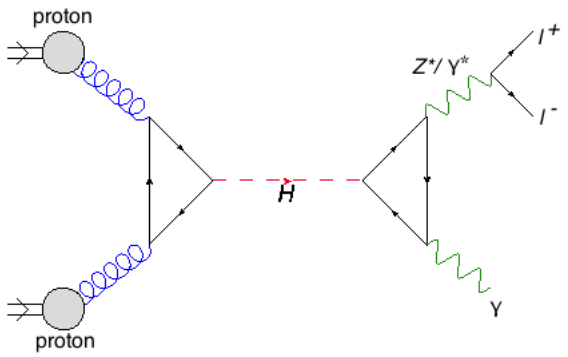

Figure 26: Feyman Diagram for Dalitz decay channel.

Note that the γ^* could also be a Z^*, in fact it is both, since it is a virtual neutral vector boson, so should have contributions from γ and Z, peaking at $m_{ll} = 0$ and $m_{ll} = 90$ GeV, but having a continuous distribution from 0 up to m_H (see figure 27). In fact, since it is a second order process, there are several one loop diagrams contributing to this channel, as shown in figure 28. The result of the contribution of all these processes can be seen in the invariant mass distribution of the produced dilepton (see figure 29), where the peaks at 0 and 90 GeV are clearly seen for electrons and for muons.

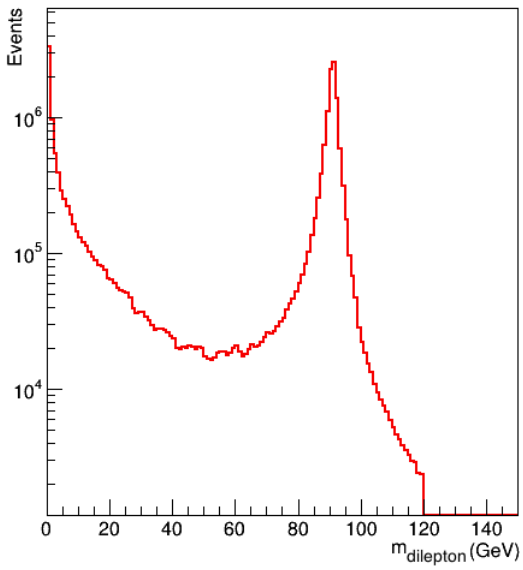

Figure 27: $H \to \gamma\gamma* \to \gamma l^+ l^-$ distribution of the invariant mass for the dilepton. The peaks are located at $m_{ll} = 0$ and $m_{ll} = 90$ GeV with a continuous distribution from 0 up to m_H (this plot was made for signal simulation using MCFM).

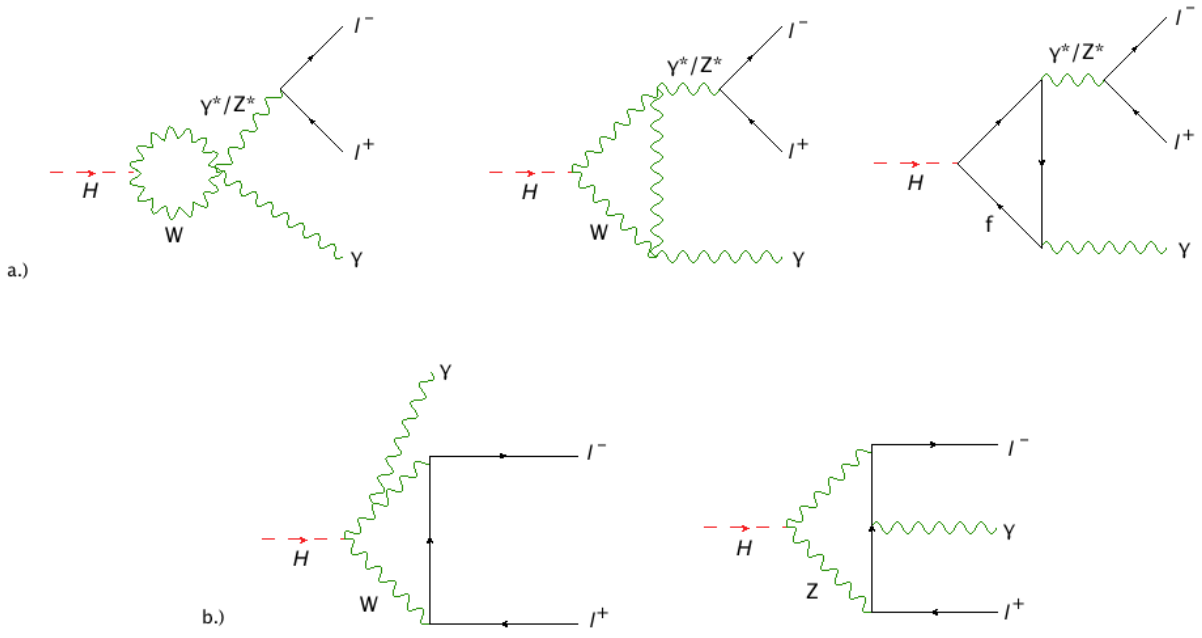

Figure 28: a.) The photon and Z pole one-loop diagrams for $H \to \gamma l^+ l^-$. b.) Four-point box diagrams for $H \to \gamma l^+ l^-$. The photon can also be radiated from another W line in the left diagram and from other charged lepton lines in both diagrams [26].

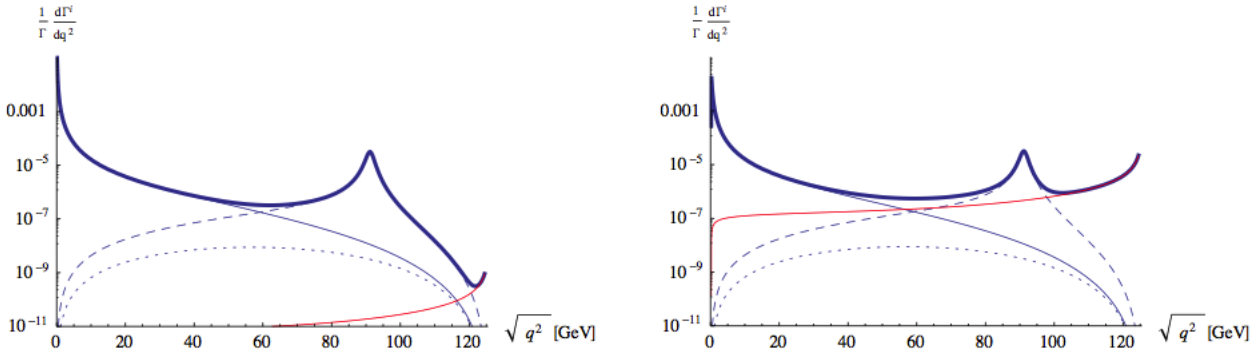

Figure 29: The invariant mass distributions of (left) $H \to \gamma e^+ e^-$ (right) $H \to \gamma \mu^+ \mu^-$ normalized by $\Gamma(H \to \gamma\gamma)$. The red line denotes the contribution of the tree diagrams, the thin solid line denotes the contribution from the γ^* pole diagrams, and the dashed line the contribution from the Z^* pole diagrams while the thick line gives the total contributions. The dotted line denotes the contribution from the four-point box diagrams [26].

Experimentally, the $H \to \gamma\gamma*$ contribution can be easily separated from the $H \to \gamma Z$ contribution by imposing a cut in the dilepton invariant mass, demanding that its value be of the order of ∼20-30 GeV; that will remove most of the contribution from Z^* decays. The first challenge of this analysis is to reconstruct dilepton events with an small invariant mass and therefore a small aperture angle, which implies getting close to the sensitivity limits of the detector. Detailed studies of the reconstruction efficiency for such dilepton events are fundamental for this analysis.

In order to link the dileptons with the Higgs one should selected events with high p_T γ's and high p_T leptons (looking for the appropriated triggers and data samples), and demand that the invariant mass of the three particles be around 125 GeV (see figure 30); this will reduce the background drastically.

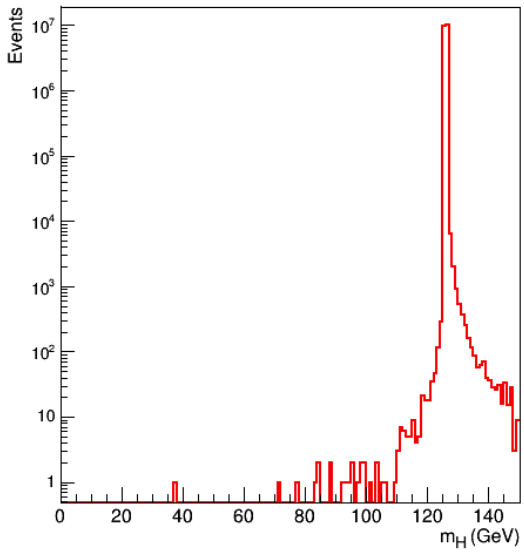

Figure 30: $H \to \gamma\gamma* \to \gamma l^+ l^-$ invariant mass of the three-body. Peak is clearly seen at $m_H = 125$ GeV (this plot was made for signal simulation using MCFM).

Next, one should demand small invariant mass for the dilepton (as already mentioned), and large aperture angle between the dilepton and the γ (see figure 31), since they should be the result of the decay of massive state, and are expected to be produced back-to-back in the center-of-mass frame of the parton-parton collision. The remaining background should be associated with dileptons producing DY processes at small q^2, accompanied by the independent emission for high p_T γ. This kind of background should be small, however the signal is also very small, so it is difficult to predicted up to which level the kinematic selection criteria can reduce this background. A similar source of background come from DY-dileptons accompanied by a high p_T jet with small multiplicity and high electromagnetic content, that can be misidentified by the detector as a γ. Once more, it is difficult to estimated how well this background can be reduced.

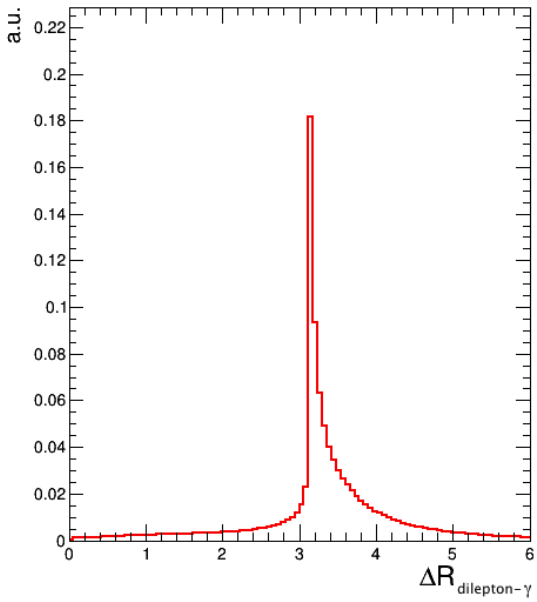

Figure 31: $H \to \gamma\gamma* \to \gamma l^+ l^-$ distribution of ΔR between the dilepton and the γ (this plot was made for signal simulation using MCFM).

In order to developed the analysis for this channel, preliminary MC studies for the signal and the background should be performed. At the moment, the only theoretical Monte Carlo that has a detailed description of this channel is MCFM [27]. However, MCFM is not included in the simulation package of CMSSW (the software framework for the CMS detector [28]). As an important part of this analysis, this issue should be addressed by me and the CMS Collaboration as a whole. After that, we should analyze the efficiency of the triggers for each channels of the Dalitz decay (e^+e^-, $\mu^+\mu^-$). In the muon channel some triggers are consider (see table 3), but for the electronic case there is not any trigger available yet. We should explore the possibility of design an appropriate HLT trigger for this channel at 14 TeV.

Trigger	Efficiency(%)	Dataset
HLT_Mu22_Photon22_CaloIdL_v*	86.1±0.4	MuEG
HLT_IsoMu24_v* HLT_IsoMu24_eta2p1_v*	81.9±0.4	SingleMu
HLT_Mu17_TkMu8_v* HLT_Mu17_Mu8_v* HLT_Mu13_Mu8_v*	5.7±0.5	DobleMu DoubleMuParked

Table 3: Summary of the usable triggers to consider in the muonic channel.

As far as the background its concerned, programs like POWHEG [29] and MADGRAPH [30] (that are included in CMSSW) can be used. In the case of the DY+jet background a full simulation including the detector effects should be performed (even at the preliminary stage). At this time there are some MC datasets for DY to LL and DY+Jets to LL, however, those datasets comprise only masses equal or greater than 10 GeV (see table 4). As we had mentioned earlier, we are interested in dileptons with small invariant masses, for this reason we should create our own MC samples in the range of 0-10 GeV.

Dataset
DYtoEE_M_10To20_TuneZ2star_8TeV_pythia6
DYtoMuMu_M_10To20_TuneZ2star_8TeV_pythia6
DY1JetstoLL_M-10To50_TuneZ2star_8TeV-madgraph

Table 4: Summary of the available Drell-Yan datasets, usable to modeling the Dalitz Background.

This background studies, and similar ones performed for 8 TeV data, should give us an indication of the level of background reduction that can be achieved, and the need or not of developing more sophisticated tools like Multivariate Analysis (MVA) or Matrix Elements Analysis (ME) to reduce the background.

Once the analysis is performed on the 8 TeV data, the tools developed for it can be adapted for the 14 TeV case and test them with simulated data in preparation for the incoming LHC run.

4 Goals

4.1 General Goals

- Search for signatures of the Dalitz decay of the Higgs boson and measurement of the branching ratio of this channel, using the data collected in 2012 by the CMS experiment during the proton-proton collision run of the LHC at the center of mass energy of 8 TeV.
- Perform Monte Carlo studies of the Dalitz decay of the Higgs boson in p-p collisions at 14 TeV in preparation for the next LHC run.

4.2 Specific Goals

- Perform Monte Carlo studies for the signal using the MCFM program [27].
- Perform background studies using POWHEG [29] and MADGRAPH [30] programs within CMSSW framework (the software of the CMS experiment) [28].
- Generate standard CMS Monte Carlo samples for the signal and background.
- Develop an analysis tool for the signal and the background for the channel.
- Identify HLT triggers and data samples at 8 TeV in order to perform the analysis developed previously.
- Determine whether or not it is necessary to develop more sophisticated background reduction techniques based on Multivariable Analysis or Matrix Element analysis for instance.
- Determine dilepton and gamma reconstruction efficiencies.
- Perform the final analysis with the 8 TeV data.
- Perform Monte Carlo studies at 14 TeV.

5 Timetable

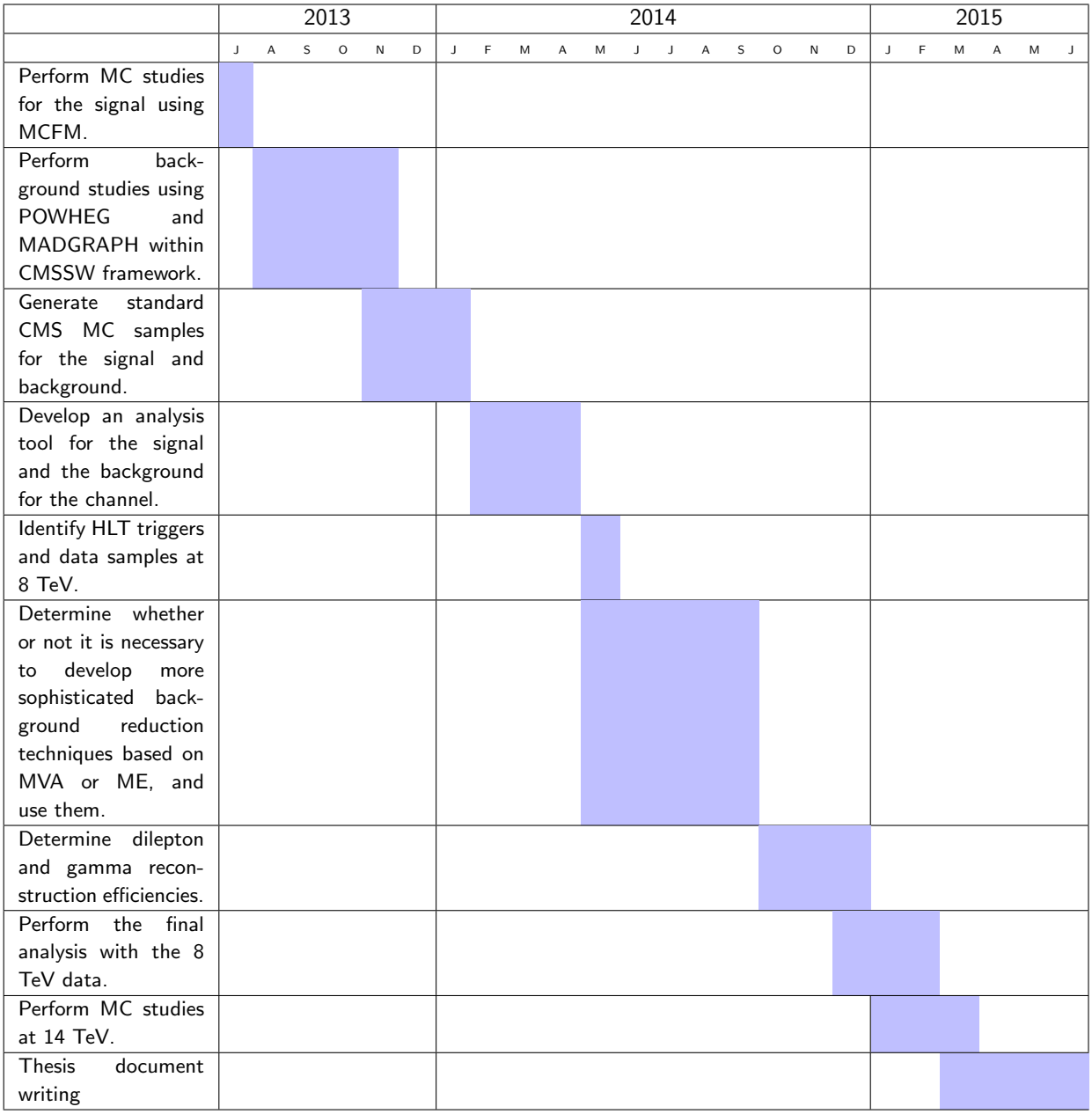
2013
2014
2015
J A S O N D J F M A M J J A S O N D J F M A M J
Perform MC studies for the signal using MCFM.
Perform background studies using POWHEG and MADGRAPH within CMSSW framework.
Generate standard CMS MC samples for the signal and background.
Develop an analysis tool for the signal and the background for the channel.
Identify HLT triggers and data samples at 8 TeV.
Determine whether or not it is necessary to develop more sophisticated background reduction techniques based on MVA or ME, and use them.
Determine dilepton and gamma reconstruction efficiencies.
Perform the final analysis with the 8 TeV data.
Perform MC studies at 14 TeV.
Thesis document writing

References

[1] CMS Collaboration. Observation of a New Boson at a Mass of 125 GeV with the CMS Experiment at the LHC. *Physics Letters B*, 716(1):30 – 61, 2012. ISSN 0370-269. doi: $10.1016/\mathrm{j.physletb.2012.08.021}$. URL `http://www.sciencedirect.com/science/article/pii/S0370269312008581`.

[2] D Orestano. Search for the standard model Higgs boson with the ATLAS detector. Technical Report ATL-PHYS-PROC-2013-063, CERN, Geneva, Mar 2013.

[3] CMS Collaboration. Observation of a New Boson with Mass Near 125 GeV in pp Collisions at $\sqrt{s} = 7$ and 8 TeV. *CMS Physics Analysis Summary*, (arXiv:1303.4571. CMS-HIG-12-036. CERN-PH-EP-2013-035), Mar 2013. Comments: Submitted to JHEP.

[4] John Ellis and Tevong You. Updated Global Analysis of Higgs Couplings. 2013.

[5] Julien Baglio and Abdelhak Djouadi. Higgs Production at the LHC. *JHEP*, 1103:055, 2011. doi: $10.1007/\mathrm{JHEP03(2011)055}$.

[6] LHC Higgs Cross Section Working Group. Handbook of LHC Higgs Cross Sections: 1. Inclusive Observables. 2011.

[7] Julien Baglio and Abdelhak Djouadi. Predictions for Higgs production at the Tevatron and the associated uncertainties. *JHEP*, 1010:064, 2010. doi: $10.1007/\mathrm{JHEP10(2010)064}$.

[8] CMS Collaboration. Combination of standard model higgs boson searches and measurements of the properties of the new boson with a mass near 125 gev. *CMS Physics Analysis Summary*, (CMS-PAS-HIG-12-045), 2012.

[9] CMS Collaboration. A new boson with a mass of 125 gev observed with the cms experiment at the large hadron collider. *Science*, 338(6114):1569–1575. 16 p, Sep 2012.

[10] ATLAS Collaboration. Measurements of the properties of the higgs-like boson in the four lepton decay channel with the atlas detector using 25 fb^{-1} of proton-proton collision data. Technical Report ATLAS-CONF-2013-013, CERN, Geneva, Mar 2013.

[11] CMS Collaboration. LHC Machine. *JINST*, 3(S08001), 2008. URL `http://iopscience.iop.org/1748-0221/3/08/S08001`.

[12] CMS public website. *CMS Luminosity-Public Results*, 2012. URL `https://twiki.cern.ch/twiki/bin/view/CMSPublic/LumiPublicResults`.

[13] CMS public website. *CMS detector design*, 2012. URL `http://cms.web.cern.ch/news/cms-detector-design`.

[14] CMS public website. *Tracker Detector*, 2012. URL `http://cms.web.cern.ch/news/trackerdetector`.

[15] CMS public website. *Electromagnetic Calorimeter*, 2012. URL `http://cms.web.cern.ch/news/electromagnetic-calorimeter`.

[16] Archana Sharma. Muon tracking and triggering with gaseous detectors and some applications. *Nuclear Instruments and Methods in Physics Research Section A: Accelerators, Spectrometers, Detectors and Associated Equipment*, 666:98 – 129, 2012. ISSN 0168-9002. doi: $10.1016/\mathrm{j.nima.2011.12.001}$. URL `http://www.sciencedirect.com/science/article/pii/S0168900211021607`.

[17] CMS public website. *Resistive Plate Chambers*, 2012. URL `http://cms.web.cern.ch/news/resistive-plate-chambers`.

[18] CMS Collaboration. Updated Measurements of the Higgs-like boson at 125 GeV in the Two Photon Decay Channel. *CMS Physics Analysis Summary*, 2013.

[19] S.Y. Choi, 2 Miller, D.J., M.M. Muhlleitner, and P.M. Zerwas. Identifying the Higgs spin and parity in decays to Z pairs. *Phys.Lett.*, B553:61–71, 2003. doi: $10.1016/\mathrm{S0370\text{-}2693(02)03191\text{-}X}$.

[20] CMS Collaboration. Properties of the Higgs-like boson in the decay $H \to ZZ \to 4l$ in pp collisions at $\sqrt{s} = 7$ and 8 TeV. *CMS Physics Analysis Summary*, 2013.

[21] CMS Collaboration. Update on the search for the Standard Model Higgs boson in pp collisions at the LHC Decaying to W^+W^- in the fully Leptonic Final State. *CMS Physics Analysis Summary*, 2013.

[22] CMS Collaboration. Search for neutral Higgs bosons decaying to τ pairs in pp collisions at $\sqrt{s} = 7$ TeV. *Phys.Lett.*, B713:68–90, 2012. doi: $10.1016/\mathrm{j.physletb.2012.05.028}$.

[23] CMS Collaboration. Search for the Standard-Model Higgs boson decaying to tau pairs in proton-proton collisions at $\sqrt{s} = 7$ and 8 TeV. *CMS Physics Analysis Summary*, 2013.

[24] CMS Collaboration. Search for a Higgs boson decaying into a b-quark pair and produced in association with b quarks in proton-proton collisions at 7 TeV. *CMS Physics Analysis Summary*, 2013.

[25] CMS Collaboration. Search for the standard model Higgs boson in the Z boson plus a photon channel in pp collisions at $\sqrt{s} = 7$ and 8 TeV. *CMS Physics Analysis Summary*, (CMS-PAS-HIG-13-006), 2013.

[26] Yi Sun, Hao-Ran Chang, and Dao-Neng Gao. Higgs decays to gamma l+ l- in the standard model. 2013.

[27] Ciaran Williams John Campbell, Keith Ellis. *MCFM - Monte Carlo for FeMtobarn processes*, 2013. URL `http://mcfm.fnal.gov/`.

[28] CMS public website. *The CMS Offline WorkBook*, 2013. URL `https://twiki.cern.ch/twiki/bin/view/CMSPublic/WorkBook`.

[29] Keith Hamilton Simone Alioli, Carlo Oleari Paolo Nason, and Emanuele Re. *The POWHEG BOX*, 2012. URL `http://powhegbox.mib.infn.it/`.

[30] Johan Alwall, Michel Herquet, Fabio Maltoni, Olivier Mattelaer, and Tim Stelzer. MadGraph 5 : Going Beyond. *JHEP*, 1106:128, 2011. doi: $10.1007/\mathrm{JHEP06(2011)128}$.